THE ASTROPHYSICAL JOURNAL, 467:126–144, 1996 August 10


# ELLIPTICALS WITH KINEMATICALLY DISTINCT CORES: WFPC2 IMAGING OF GLOBULAR CLUSTERS[1]

DUNCAN A. FORBES
Lick Observatory, University of California, Santa Cruz, CA 95064; forbes@lick.ucsc.edu
MARIJN FRANX
Kapteyn Institute, University of Groningen, P.O. Box 800, 9700 AV Groningen, The Netherlands; franx@astro.rug.nl
GARTH D. ILLINGWORTH
Lick Observatory, University of California, Santa Cruz, CA 95064; gdi@lick.ucsc.edu
AND
C. M. CAROLLO
Leiden Observatory, 2300 RA Leiden, The Netherlands; carollo@strw.leidenuniv.nl
*Received 1996 January 2; accepted 1996 February 27*

## ABSTRACT

New globular clusters may form in the merger of two galaxies. Perhaps the best examples of merger remnants are the set of ellipticals with kinematically distinct cores. Here we present *Hubble Space Telescope* (*HST*) Wide Field and Planetary Camera 2 (WFPC2) imaging of 14 kinematically distinct core ellipticals to examine their globular cluster systems. In particular, we probe the galaxy central regions, for which we might expect to see the strongest signatures of some formation and destruction processes. These data increase substantially the number of extragalactic globular cluster systems studied to date. We have developed a method for galaxy subtraction and selection of globular clusters which results in about 200 globulars per galaxy to a limiting magnitude of $V \sim 25$. Simulations of artificial globulars are described also.

We find that the globular cluster luminosity, and color, vary only weakly, if at all, with galactocentric distance. The mean colors of globular clusters are constant with globular cluster magnitude. Several clear trends are also present. First, globular cluster colors are bluer (more metal poor by $\sim$0.5 dex) than the underlying galaxy starlight at any given galactocentric distance. Second, we find a good correlation over roughly 10 magnitudes between the mean globular cluster metallicity and parent galaxy luminosity of the form $Z \propto L^{0.4}$. This relationship includes dwarf ellipticals, spiral galaxy bulges, and giant ellipticals. Third, we find that globular cluster surface density distribution can be described by a core model, for which the core radius correlates with galaxy luminosity. Last, for the sample as a whole, the globular cluster systems are closely aligned with the galaxy major axis and are slightly rounder than the galaxy itself, although their are some notable exceptions.

Our results favor scenarios in which ellipticals form from massive, gas rich progenitors at early epochs. Detailed simulations of the formation of globular cluster systems would be valuable to draw firmer conclusions.

*Subject headings:* galaxies: elliptical and lenticular, cD — galaxies: kinematics and dynamics — galaxies: nuclei — galaxies: star clusters

## 1. INTRODUCTION

Globular clusters, as well as being interesting in their own right, provide important clues to the formation and evolution of their parent galaxy (see, for example, Harris 1991, and references therein). In particular, the merger of two spiral galaxies may lead to the formation of an elliptical galaxy and create an additional population of globular clusters (GCs) in the process (Schweizer 1987). This potentially overcomes the objection raised by van den Bergh (1990) that ellipticals have many more GCs, per unit light, than expected from simply combining the observed GC population of two spirals. This idea was expanded upon by Ashman & Zepf (1992). In their model, new GCs are formed in massive gas clouds from the progenitor spirals. These gas clouds are of higher metallicity and are more centrally concentrated than the original GCs belonging to the spirals. Thus, an observational consequence of such a model is a radial metallicity gradient and at least two peaks in the metallicity distribution of the resultant GC population.

Kinematically distinct core (KDC) ellipticals have central regions that rotate rapidly, and often in an opposite direction, compared to the stars in the outer parts of the galaxy. They are found in about one-third of all ellipticals and are generally thought to be the result of a merger (Illingworth & Franx 1989). This merger may involve the accretion of a small secondary (Balcells & Quinn 1990), although this model has difficulty explaining the metallicity (Bender & Surma 1992) and surface brightness (Forbes, Franx, & Illingworth 1995) profiles of some KDC galaxies. A more plausible alternative involves the merger of gas-rich galaxies in which gas dissipates into the central regions and subsequent star formation leads to a KDC. Hernquist & Barnes (1991) have studied this for the case of two near equal-mass disk galaxies. Many KDC galaxies show evidence for small-scale dust lanes and rings (Forbes et al. 1995), further supporting the idea that these galaxies have accreted material. Thus, KDC galaxies offer an ideal sample

[1] Based on observations with the NASA/ESA *Hubble Space Telescope*, obtained at the Space Telescope Science Institute, which is operated by AURA, Inc., under NASA contract NAS 5-26555.

in which to study their GC population and examine critically the hypothesis of merger-induced GC formation. In addition, such ellipticals cover a range of environments (which may affect the relative number of GCs and metallicity; Harris 1991) and X-ray luminosities (which could contribute to GC formation via a cooling flow; Fabian, Nulsen, & Canizares 1984). The results for KDC ellipticals may also be applicable to other elliptical galaxies, as our WFPC1 study indicated that the photometric properties of KDC ellipticals follow the same scaling relations as "kinematically normal" ellipticals (Forbes et al. 1995).

Previous studies of GC systems in kinematically distinct core galaxies have included NGC 4278 (Harris & van den Bergh 1981), NGC 4365 (Harris et al. 1991), NGC 4406 (Hanes 1977), NGC 4472 (Harris et al. 1986; Couture, Harris, & Allwright 1991), and the work of Ajhar, Blakeslee, & Tonry (1994), who studied NGC 4365, NGC 4406, NGC 4472, and NGC 4552. However, these ground-based studies, and those of others, are limited to relatively large galactocentric radii by seeing and blending effects, whereas we might expect the inner regions to have the strongest signatures of some formation and destruction mechanisms. In a review, Harris (1993) stated that ". . . essentially nothing is known about the inner globular clusters in most galaxies, and much new observational work could be done in this direction."

Here we present F555W ($V$) and F814W ($I$) Wide Field and Planetary Camera 2 (WFPC2) images of 14 ellipticals with well-established KDCs. The superior resolution of *HST* makes it possible to probe GC properties within one effective radius of the parent galaxy. To date only two other ellipticals, NGC 4881 (Baum et al. 1995) and M87 (Elson & Santiago 1995; Whitmore et al. 1995), have published WFPC2 data on their GC system. We examine the magnitude, color, and spatial distributions of the GC system in the central few kpc of each galaxy. Results for the parent galaxies themselves, and implications for the formation mechanisms of KDCs, will be presented elsewhere (Carollo et al. 1996). We assume $h = H_0/100$ km s$^{-1}$ Mpc$^{-1}$ throughout this paper, although in a future paper we will discuss the use of our GC luminosity functions for the derivation of the Hubble constant.

## 2. OBSERVATIONS AND INITIAL DATA REDUCTION

A total of 14 kinematically distinct core galaxies were observed with *HST*'s WFPC2 between 1994 April and November. These galaxies represent most of the well-established cases known to date. Their properties are summarized in Table 1. Data for each galaxy consist of a pair of 500 s F555W images and a pair of 230 s F814W images. The nucleus of each galaxy is located near the center of the PC CCD. All four CCDs are 800 × 800 pixels, with a scale of 0".046 pixel$^{-1}$ for the PC and 0".097 pixel$^{-1}$ for the WFC CCD.

The standard Space Telescope Science Institute (STScI) pipeline was used for the initial data reduction. Before combining each pair of images, we needed to check the relative alignment. We find that each pair of F555W and F814W images is aligned to within less than 0.1 WFC pixel ($<$0".01), and so they can be combined without any shifting. Each pair of images is combined using the STSDAS task CRREJ, which has been modified by J. Biretta for WFPC2 images. The raw frames contain a large number of cosmic rays, hot pixels, and cold pixels. Hot pixels are created at a rate of hundreds per month (Holtzman et al. 1995a) and tend to be single-pixel events, whereas cold pixels (CCD traps) are more stable with time. The combining task does a very good job of removing cosmic rays and to some extent hot pixels (see discussion below). Using lists of CCD traps kindly supplied by the WFPC2 group at STScI, we have interpolated over all such pixels. We have also trimmed each image to exclude the "obscured region" near the pyramid edges, yielding 751 × 751 pixel images. The final trimmed images are missing less than 1% of the effective area because the WFPC2 field of view actually overlaps each CCD by about 40 pixels.

We then made a first-order attempt to remove the galaxy background. For the WFC images, there is a slight background gradient which is strongest toward the direction of the pyramid center (which is the direction of the galaxy center). This gradient is largely removed by a bi-cubic spline fit. For the PC image, we fitted the galaxy isophotes using the STSDAS task ELLIPSE (see Forbes & Thomson 1992). By subtracting these models, we are left with globular clus-

TABLE 1

GALAXY PARAMETERS

| Galaxy (1) | Type (RC2) (2) | Group (3) | Distance ($h^{-1}$ Mpc) (4) | $r_{\rm eff}$ ($h^{-1}$ kpc) (5) | $M_V$ (mag + 5 log $h$) (6) | $B-V_0$ (mag) (7) | $A_V$ (mag) (8) | log $L_X$ ($h^{-2}$ ergs s$^{-1}$) (9) |
|---|---|---|---|---|---|---|---|---|
| NGC 1427..... | E5 | Loose (23) | 13.2 | 2.53 | −19.77 | 0.93 | 0.00 | ... |
| NGC 1439..... | E1 | Loose (21) | 15.5 | 3.13 | −19.81 | 0.93 | 0.05 | ... |
| NGC 1700..... | E4 | Loose (6) | 40.6 | 2.72 | −21.71 | 0.93 | 0.09 | ... |
| NGC 3608..... | E2 | Loose (30) | 10.2 | 1.76 | −19.29 | 0.98 | 0.00 | 39.19 |
| NGC 4278..... | E1 | Coma I | 7.3 | 1.17 | −19.26 | 0.96 | 0.08 | ... |
| NGC 4365..... | E3 | Virgo ? | 10.4 | 2.82 | −20.42 | 0.99 | 0.00 | 39.48 |
| NGC 4406..... | E3 | Virgo | 10.4 | 4.50 | −21.09 | 0.89 | 0.08 | 40.75 |
| NGC 4494..... | E1 | Loose (170) | 11.2 | 2.49 | −20.46 | 0.90 | 0.05 | ... |
| NGC 4589..... | E2 | Loose (13) | 18.3 | 3.71 | −20.66 | 0.94 | 0.03 | 39.88 |
| NGC 5322..... | E3 | Loose (13) | 21.1 | 3.63 | −21.42 | 0.89 | 0.00 | 39.93 |
| NGC 5813..... | E1 | Loose (11) | 15.9 | 4.39 | −20.56 | 0.94 | 0.11 | ... |
| NGC 5982..... | E3 | Loose (5) | 29.9 | 2.07 | −21.35 | 0.95 | 0.02 | 40.45 |
| NGC 7626..... | E1P | Loose (8) | 37.2 | 6.85 | −21.86 | 1.00 | 0.12 | 40.82 |
| IC 1459 ..... | E3 | Loose (10) | 16.6 | 3.13 | −21.20 | 0.99 | 0.03 | 40.45 |

NOTE.—(1) Galaxy name; (2) morphological type from RC2; (3) galaxy environment such as a loose group (number of bright galaxies in the group) or cluster; (4) distance from Bender, Burstein, & Faber 1992 (BBF) or Faber et al. 1989; (5) effective radius from BBF, Goudfrooij et al. 1994, or Bender et al. 1989; (6) absolute $V$ magnitude from Faber et al. 1989; (7) average $B-V_0$ color from Faber et al. 1989; (8) extinction $A_V$ from Faber et al. 1989 assuming $A_V = 0.75\ A_B$; (9) X-ray luminosity from Roberts et al. 1991.

ters, foreground stars, small faint galaxies, and possibly dust features at the center of the galaxy. An example of a background-subtracted F555W image for NGC 1427 is shown in Figure 1 (Plate 1). Most of the objects are globular clusters, and similar numbers appear on each image (for the PC image, the increased cluster density roughly compensates for the reduced areal coverage).

### 2.1. *Globular Cluster Selection and Measurement*

The selection and photometry of GCs is carried out using the IRAF version of DAOPHOT (Stetson 1987). Selection of objects is based on the F555W image, which has a higher signal-to-noise ratio (S/N) than the F814W image for the objects of interest. The same DAOFIND parameters are used for each galaxy. In particular, we use roundness parameters $-0.5$ to 0.5 and a threshold in counts of 4 DN (data numbers) for the PC and 5 DN for WFC images. We have adopted a fairly tight shape constraint so that the detected objects are not too distorted by noise or nearby dust features, which may also affect their magnitudes and colors. The disadvantage of this approach is that a few faint sources, that are probably real GCs, will not be detected by DAOPHOT, although measurement of these objects would give spurious results and so they would be rejected from the subsequent analysis anyway. Tests on actual WFC images indicates that to $V = 25$, $\sim 10\%$ of detected sources are more elongated than our roundness criterion. Visual inspection of these sources suggests that about half (5%) are clearly not GCs, i.e., they are noise, diffraction spikes of stars, or galaxies. Thus, we are excluding less than 5% of GCs with our conservative roundness criterion. A similar situation is present for PC images in which there is no dust. For the dusty galaxies, DAOPHOT detects many sources more elongated than our roundness constraint. Here it is more difficult to make conclusive statements; however, a visual inspection of these images suggests that DAOPHOT is only missing a small numer (approximately five per galaxy) of possible GCs to $V = 25$. The colors of GCs located at the edges of dust patches is discussed in § 4.4.

For the PC image, the limiting magnitude for point sources is about 0.3 mag brighter than for the WFC images (Burrows et al. 1993). To compensate for this, we chose a slightly lower count threshold for the detection of objects, i.e., 4 DN instead of 5 DN. In order to confirm that all four CCDs have similar detection characteristics, we have combined the objects detected by DAOPHOT for NGC 4365 and NGC 5982 (the only two galaxies in the sample with no obvious dust in the PC or WFC frames). We find that each CCD has a similar detection fraction of objects $V = 25$.

We also tested an alternative method of selecting objects independently on both the F814W and F555W images, and including only those objects in common to give an object list. This method gave significantly fewer objects at faint magnitudes because the F555W image has a higher effective S/N for GCs than the F814W image. We believe that the additional faint objects (found using the selection in the F555W image only method) are real detections, as their mean color is indistinguishable from that of the brighter sources.

Photometry of the detected objects is carried out for both the F814W and F555W images using the coordinates of the objects selected from the F555W image. Any residual background counts remaining from the background fits are removed by doing "sky" subtraction in an annulus around each object. We have chosen to measure magnitudes in a small aperture and make aperture corrections in order to reduce the noise from the background in very large apertures (the WFPC2 PSF actually contains some light out to 30 WFC pixels). The optimum aperture for stars has been determined by several workers to be 2–3 WFC pixels in radius (Whitmore 1995). Our tests of the scatter in $V-I$ color of actual GCs indicates that to $V = 25$ the dispersions between 2 and 3 pixel apertures deviate by less than 5% (in the sense that the 2 pixel aperture has a smaller dispersion). However, with the 2 pixel apertures, there are several issues that may cause a systematic bias in the final photometry, such as centering, small area calculations, and the largely unknown variation of aperture corrections with position on the CCD. We have taken what we believe to be the conservative approach and used 3 pixel radius apertures. These aperture magnitudes are converted to total magnitudes using the encircled energy tables of Holtzman et al. (1995a), i.e., for F555W the correction is 0.23 and 0.16 mag for the PC and WFC CCDs, respectively, and for F814W, 0.32 and 0.16 mag. These aperture corrections are within 0.05 mag of those used by Whitmore et al. (1995) based on measurements of isolated stars. The geometric distortion between F555W and F814W is negligible. In order to convert WFPC2 flight magnitudes to a ground-based standard photometric system, we use (Holtzman et al. 1995b)

$$V = 21.724 - 2.5 \log (\mathrm{DN/s}) - 0.052(V-I) + 0.027(V-I)^2 , \quad (1)$$

$$I = 20.840 - 2.5 \log (\mathrm{DN/s}) - 0.063(V-I) + 0.025(V-I)^2 . \quad (2)$$

These equations are for a gain setting of 15, which applies to all but three of our galaxies (we added 0.745 mag to the zero points for gain setting 7). Assuming $(V-I) = (\mathrm{F555W\ magnitude} - \mathrm{F814W\ magnitude})$ in the above relations introduces a rms error of less than 1.5% in the final magnitude determination given the range of GC colors. Finally, we have corrected the magnitudes for Galactic extinction, listed in Table 1. We have restricted the detected magnitude range to $19 < V < 26$, as there appear to be no GCs brighter than $V \sim 20$ (brighter sources appear to be stars) and fainter than $V \sim 25$ (this is our effective limiting magnitude and will be discussed further in the next section).

For each selected object, we have fitted the profile with a Gaussian and measured its FWHM size, determined R.A. and declination positions using the STSDAS task METRIC, and calculated position angle on the sky and the radial distance from the galaxy center. Thus, we now have a list of position, $V$ magnitude and its error, $I$ magnitude and its error, $V-I$ color and its error from a quadrature sum of the photometric errors, size, position angle, and galactocentric distance for each object.

At this point, the list may include hot pixels, foreground stars, and faint galaxies as well as globular clusters. Hot pixels can be effectively excluded by comparing the positions of detected objects (in pixel coordinates) to the location of known hot pixels shortly after the galaxy observation date. These known hot pixels should be a superset of the hot pixels for our actual data. The exception might be NGC 1700, which was observed on 1994 April 17 before the April 23 thermal cycling (we rely on object sizes and colors to check the reality of selected objects for this

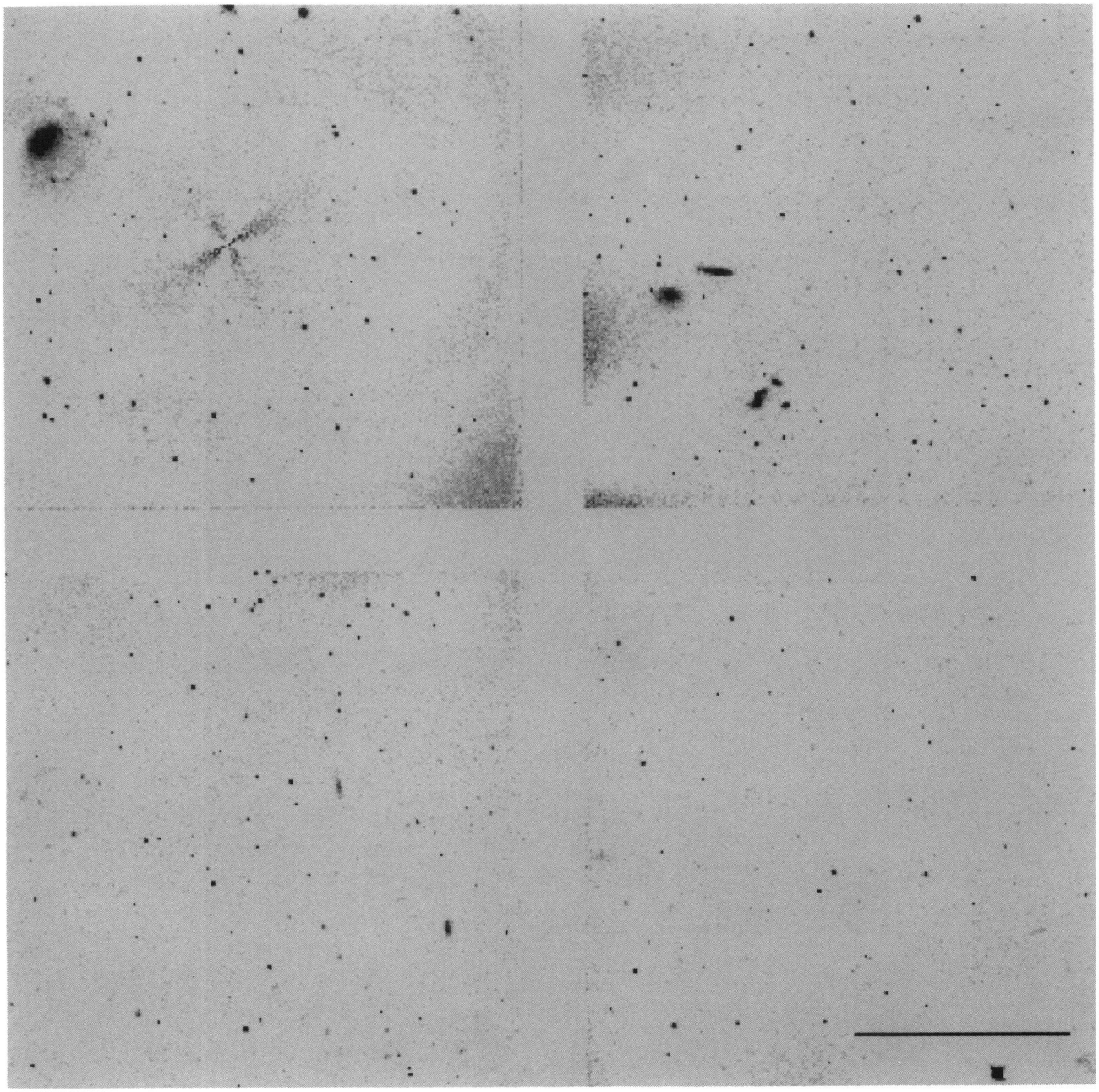

FIG. 1.—Gray-scale WFPC2 image of NGC 1427 after galaxy subtraction. The blank region between CCDs has been removed, as this is in the pyramid shadow. Here the PC CCD is shown full size (*top left*), even though its area coverage is only a quarter that of the WFC CCDs. The horizontal bar in the bottom right represents a WFC scale of 30″. The image reveals over 150 globular clusters with magnitudes $19 < V < 25$.

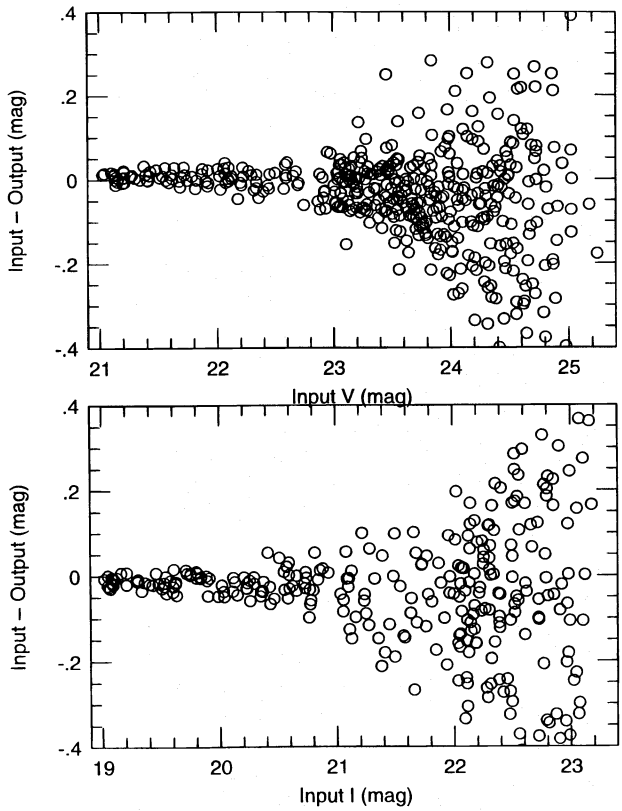


FIG. 2.—Photometric errors from simulations. The difference between the input magnitude of the simulated globular cluster and that measured by DAOPHOT is shown against input magnitude. A photometric error of $\pm 0.1$ mag is reached at $V \sim 24$ and $I \sim 22$.

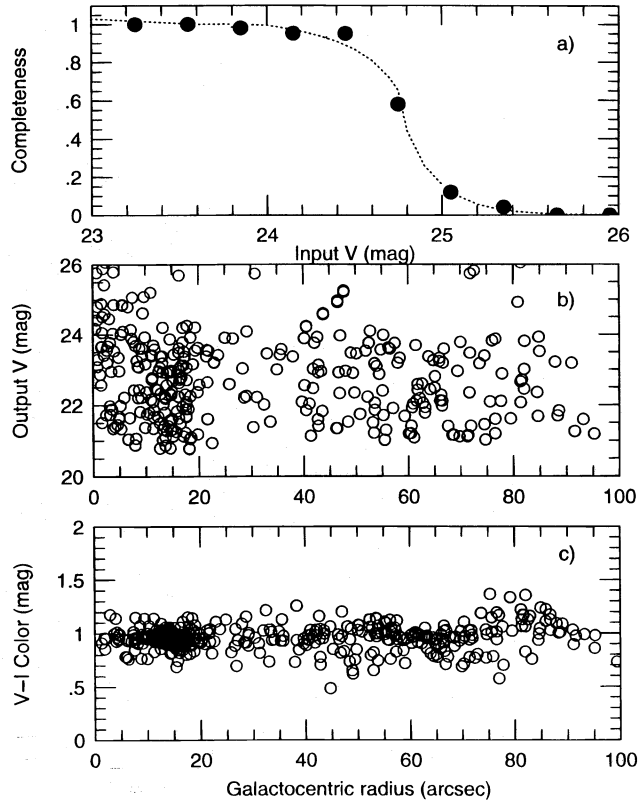


FIG. 3.—(*a*) Completeness function from simulations. The fraction of recovered globular clusters is shown against input magnitude. A fit to the completeness function is shown by a dashed line. The 100% completeness level is $V \sim 24$. (*b*) Variation of the output globular cluster $V$ magnitude as a function of galactocentric radius from simulations. (*c*) Radial variation of output $V-I$ color (a value of 1.0 was inputted). There are no intrinsic radial gradients in magnitude or color for simulated globular clusters.

galaxy). We have checked to see if any hot pixels lie within 3 pixels of our selected objects and typically find only half a dozen coincidences per galaxy. These objects are then removed from the list.

Elson & Santiago (1995) estimate that a typical high galactic latitude field contains about two foreground stars per WFC image in the magnitude range $20 < V < 26$. The PC image contains a smaller number. Thus contamination by foreground stars is very small. Furthermore, we have removed all objects with FWHM size $\geq 3.0$ pixels (typically five per image). This is about the size expected for the large Galactic globular cluster Omega Cen if it were placed at Virgo distance ($h = 0.75$) and convolved with *HST*'s point-spread function (PSF) (Grillmair 1995). Thus, for intrinsically smaller globulars or ellipticals more distant than Virgo, the expected globular size is less than 3 PC pixels. Visual inspection reveals that most objects with sizes greater than 3 pixels are probably background galaxies. Studies of random high galactic latitude WFPC2 fields suggest that the number of small (FWHM < 3 pixels) galaxies to $I = 22$ ($V \sim 23.5$) is perhaps only one or two per WFC CCD image (Forbes et al. 1994; Phillips et al. 1995). Galaxies fainter than $V = 24$ are in general not detected in these images.

### 2.2. *Errors and Completeness Tests*

Photometric errors and sample completeness have been estimated in a manner similar to that described by Secker & Harris (1993). Using the IRAF task PSF, we created an artificial object from the average shape of ~20 real GCs. This was done for both filters in a WFC image. Then we populated a relatively empty image (the few existing GCs are interpolated across) with artificial GCs. The noise characteristics of this image are fairly representative for all galaxies. The objects were placed at random locations, using the task ADDSTAR, in 1 mag bins to cover the range $21 < V < 25.5$. Objects in the $I$ images were generated at the same position as in the $V$ images with an input color of $V-I = 1.0$. Several hundred artificial GCs were created, but no more than 150 per image to ensure that blending of objects did not occur (of the total available area, 150 GCs covers less than 1%). Even for the richest GC systems in our sample, there is no evidence of blending. The next step is to find and measure magnitudes of these artificial GCs. This is done using DAOPHOT with the same selection and photometry parameters as for the real data.

In Figure 2 we plot the difference in the actual input magnitude of the artificial GC and its measured magnitude as a function of input magnitude. This gives us an estimate of the measurement, or photometric error, for our sample. The photometric error is fairly symmetric about zero, showing that random errors dominate over any systematic bias. Taking the absolute value of the error, we fit an exponential of the form

$$\mathrm{pe}(m) = \exp\,[a(m - b)]\,, \qquad (3)$$

to describe the photometric error. Here pe is the absolute value of the input minus output magnitude, $m$ is the GC magnitude and $a$ and $b$ are coefficients. For the $V$-band data, we find that $a = 0.83$ and $b = 26.84$, and for the $I$-band data $a = 1.07$ and $b = 23.99$. This gives a photometric error of 0.1 mag at $V \sim 24$ and $I \sim 22$. We can compare these error functions to the measurement errors determined directly by DAOPHOT for the real GCs. Reassuringly, the variation of the measurement error with magnitude is very similar to that determined from our tests described above. This gives us confidence in the magnitude and color errors given by DAOPHOT.

Although we will not discuss GC luminosity functions, it is still of interest to determine the completeness function for our data, i.e., quantify the ability of DAOPHOT to detect GCs as a function of magnitude. Here we use the same input lists of artificial GCs as above, but now we consider whether each added GC was recovered by DAOPHOT. The ratio of the number of input objects to those detected gives the sample completeness. The $V$ completeness function (cf) for a WFC image is shown in Figure 3*a*. We find that our sample is essentially 100% complete to $V \sim 24$ and that our detection limit is $V \sim 25$. The cf is fitted over the range of interest with two exponentials. The first, $\mathrm{cf}(m) = a \exp [b/(m - c)]$ is fitted to magnitudes brighter than the 50% completeness level and $\mathrm{cf}(m) = a/\exp [b(m - c)]$ is fitted to magnitudes fainter than the 50% level, where $a$, $b$, and $c$ are coefficients. At the 50% completeness level, these functions agree within $\pm 0.03$ mag. To first order, we would expect all four CCDs to have a similar completeness function, since the detection rate as a function of magnitude is similar for each CCD.

## 3. RESULTS

### 3.1. *Simulations*

Before presenting the real data, we need to check whether our detection and photometry procedure has introduced any obvious bias. As mentioned earlier, the variation of DAOPHOT computed photometric errors with total magnitude is consistent with that from the simulations. It is possible that our procedure introduces a detection or photometric bias that depends on distance from the galaxy center. In Figures 3*b* and 3*c*, we show the radial $V$ magnitude and $V-I$ color profiles using the same detection and photometry methods as for the real data. The $V$ magnitudes of the simulated GCs were distributed randomly between $V = 21$ and $V = 26$, while the $I$ magnitudes were set to be $I = V - 1.0$. We find that the simulated GCs do *not* show a trend with galactocentric radius in either magnitude or color. Thus, any statistically significant radial gradients seen in the actual WFPC2 data are likely to be real.

### 3.2. *Globular Clusters*

Color-magnitude diagrams for the sample galaxies are presented in Figure 4. These show that most galaxies reveal a relatively tight concentration of points around $V-I \sim 1$ and that this average color is relatively constant with magnitude. The dispersion in color increases at faint magnitudes. At the detection limit, we would expect the average color to become redder, as we are biased against detecting blue objects, but this is not seen due to our conservative magnitude cutoff. The raw (i.e., not corrected for incompleteness) globular cluster luminosity functions (GCLFs) are shown in Figure 5. A variety of shapes are seen. For some galaxies, the expected apparent magnitude peak in the GCLF, if it is universal, is within our completeness limit (e.g., NGC 4278), while for others it is well beyond (e.g., NGC 1700). Globular cluster luminosity functions corrected for incompleteness will be discussed in a future paper. The distribution of globular cluster colors for our sample is shown in Figure 6. These histograms show that there is a fairly small range in the mean GC color from galaxy to galaxy.

At this stage, we have decided to apply an additional selection criterion based on GC color. For the subsequent results and analysis given below, we will restrict the data set for each galaxy to GCs with colors within 3 $\sigma$ of the mean. This should remove any objects with deviant colors that are due to undetected cosmic rays or noise spikes. Such a selection process removes typically only a small fraction of objects from the list. Nevertheless, we have checked the rejected objects to ensure that we are not excluding the most interesting candidates. Objects with extreme red or blue colors do *not* lie preferentially at small or large galactocentric distances, so we are not, for example, removing centrally located blue GCs. The objects with extreme colors tend also to be the faintest sources (see Fig. 4), suggesting that photometric errors play a large role in determining their deviant colors. We are confident that our final list does not contain any hot pixels or resolved galaxies and that the contribution from cosmic rays, foreground stars, and unresolved galaxies is negligible.

After applying this 3 $\sigma$ rejection, we give a summary of the GC system properties for each galaxy in Table 2. The number of GCs per galaxy ranges from 39 (NGC 1700) to 328 (NGC 4365). For the sample as a whole, the mean color is $V-I = 1.09$. Assuming that $V-I$ colors correspond to metallicity, we include also in Table 2 the inferred metallicity using the relation from Couture, Harris, & Allwright (1900), i.e.,

$$[\mathrm{Fe/H}] = 5.051(V-I) - 6.096 . \quad (4)$$

Next we examine the projected radial distribution of GC magnitude, color, and surface density. Globular cluster magnitude as a function of galactocentric radius is plotted in Figure 7. Most galaxies are consistent with no mean GC magnitude variation with distance from the galaxy center. We note that there are slight differences for some galaxies; for example, NGC 4494 appears to have a small enhancement of bright GCs in the central kiloparsec, whereas for NGC 5982 they seem to be lacking.

In Figure 8 we show the radial distribution of GC color. We have fitted a linear regression line over the full range of galactocentric radius for each galaxy. An iterative fit was performed, with each data point inversely weighted by its error from DAOPHOT (which gives less weight to fainter GCs). The slopes are listed in Table 2. Most of the sample galaxies show little, or no, evidence for a GC color gradient with galactocentric radius. There are six galaxies which show weak radial color gradients. We show also in Figure 8 the color gradient of the underlying galaxy at small radii from Carollo et al. (1996). Although the GC colors overlap with that of the galaxy starlight, the GC colors are systematically bluer on average than the galaxy itself. The difference for the whole sample is $\Delta(V-I) \sim 0.10 \pm 0.06$.

We show the surface density, per kpc$^2$, of GCs with galactocentric radius in Figure 9. The GC counts have been restricted to position angles covering only one hemisphere,

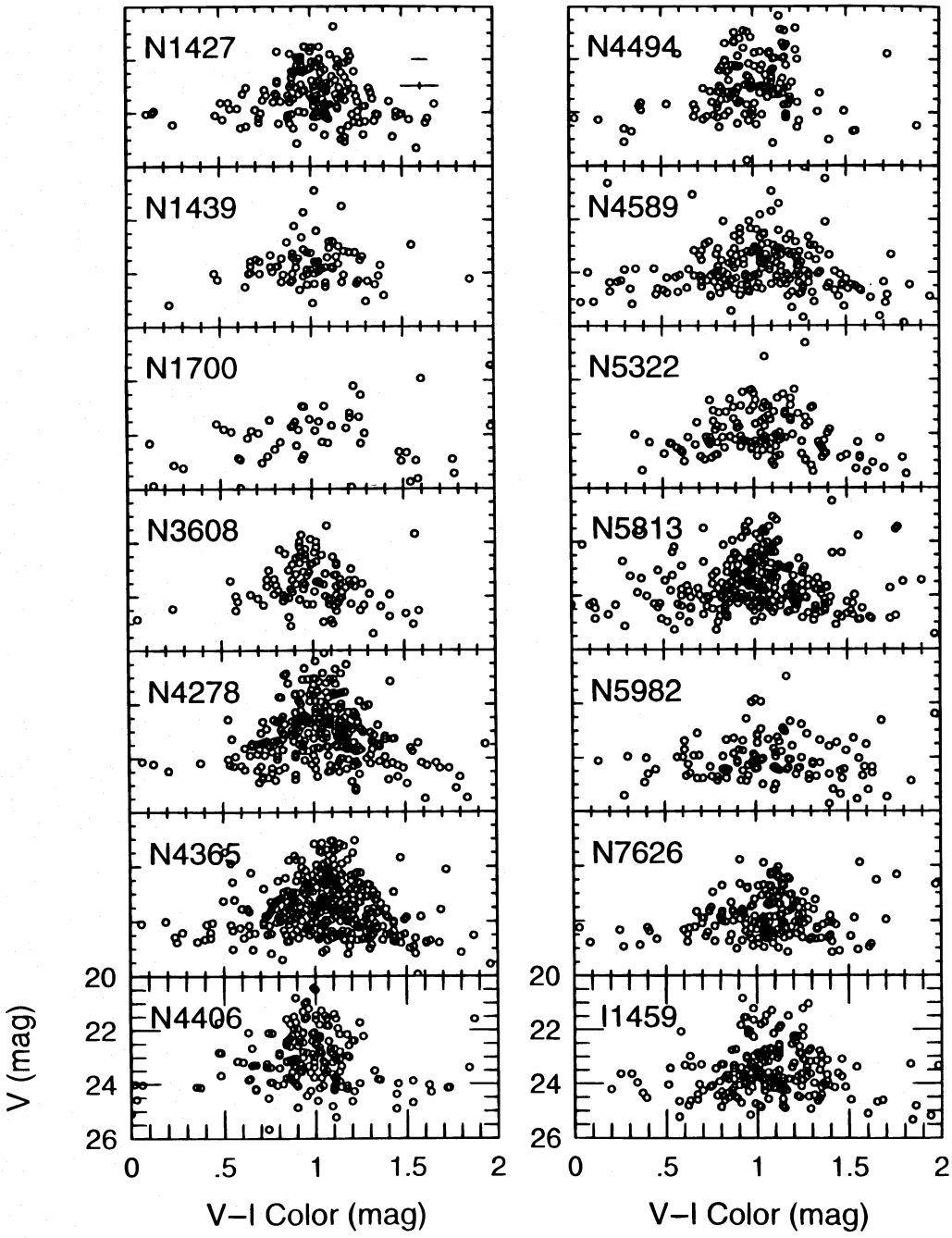


FIG. 4.—Color-magnitude diagrams for the sample galaxies. Typical error bars are shown in the top left panel. Globular cluster color is fairly constant with magnitude.

or side, of the galaxy (i.e., WFPC2 angles of V3 $\pm$ 90°). For this hemisphere, the WFPC2 field of view provides almost complete coverage (we are missing $<1\%$ of the area) out to some fixed galactocentric distance (i.e., 100″). To estimate the total surface density, we multiply the number of GCs by two. Figure 9 shows the average surface density in several annular bins with Poisson errors and the underlying galaxy light profile normalized by an arbitrary vertical offset.

The GC surface density profile for all galaxies appears to rise less steeply, than the galaxy light, toward the galaxy center. For two galaxies (NGC 5813 and IC 1459), there is even an indication that the number density falls in the central kiloparsec. In order to quantify the profiles, we have fitted a "core model" of the form $\rho = \rho_0(r_c^2 + r^2)^{-1}$. The measured core radii ($r_c$) are given in Table 2 and plotted against galaxy absolute magnitude in Figure 10. A weighted fit gives $r_c = -0.62 \pm 0.1M_V - 11.0$. A correlation is seen in the sense that more luminous galaxies have larger GC system core radii. The correlation between GC core radius and galaxy effective radius is weaker than for galaxy luminosity.

As noted above, we have almost complete areal coverage of 180°, allowing us to examine also the azimuthal distribution of GCs on one side of the galaxy. Figure 11 shows the azimuthal distribution for the sample galaxies $\pm$90° from the galaxy major axis. Some galaxies show high counts

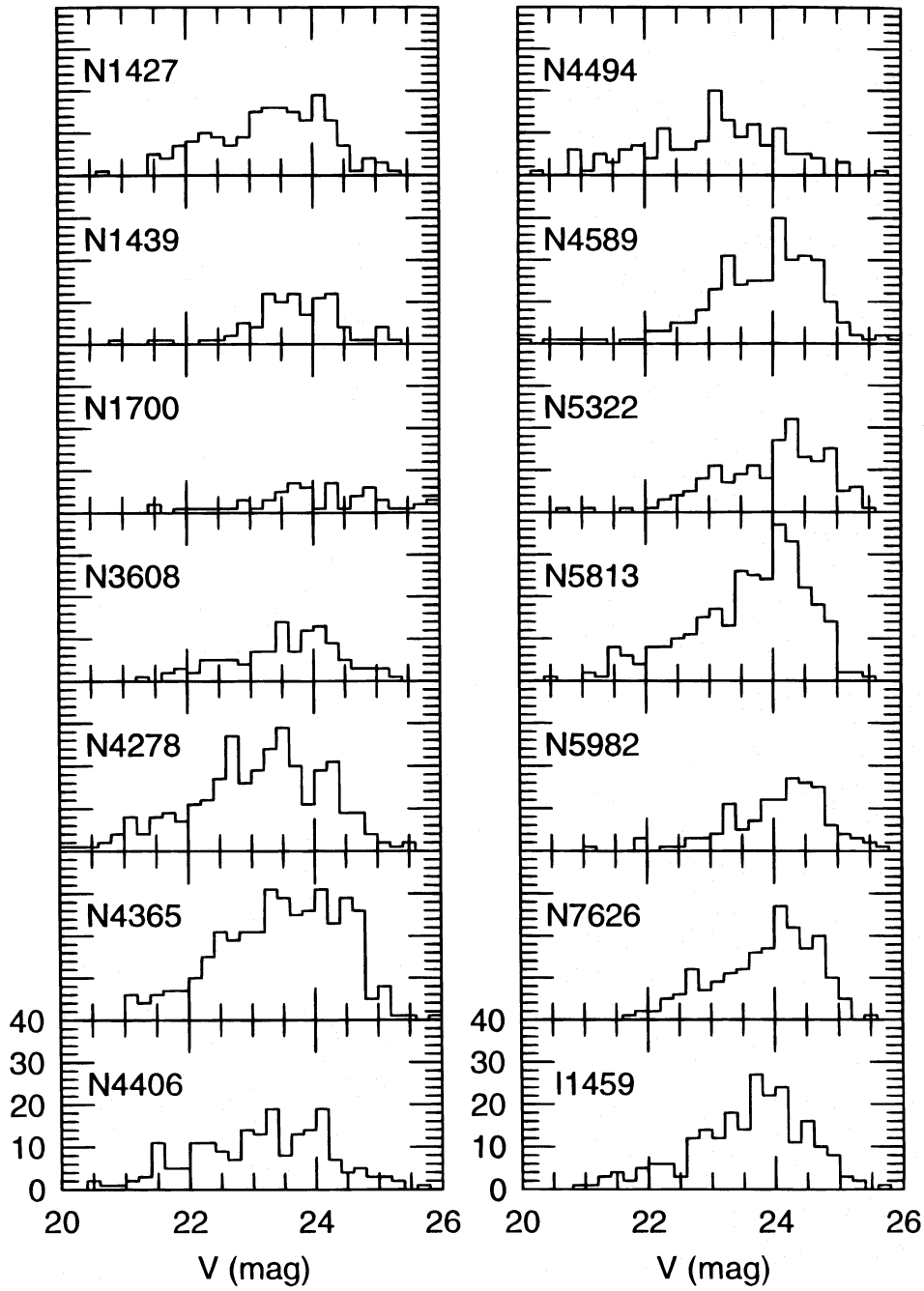


FIG. 5.—Globular cluster luminosity functions for the sample galaxies. The luminosity functions have not been corrected for completeness effects.

close to 0°, indicating that the GC system is closely aligned with the galaxy major axis.

## 4. DISCUSSION

### 4.1. *Comparison with Ground-based Data*

Three of the galaxies in our sample have had their GC systems studied previously using ground-based data. The single-filter photographic studies of NGC 4278 (Harris & van den Bergh 1981) and NGC 4406 (Hanes 1977; Cohen 1988) and the CCD study of NGC 4365 (Harris et al. 1991) generally concentrated on GCLFs and their usefulness as distance indicators. Harris (1991) quotes a specific frequency ($S_N$) for these galaxies of 6.1 for NGC 4278, 7.7 for NGC 4365, and 5.4 for NGC 4406 (Harris assumed $h = 0.75$). The specific frequency is a measure of the relative richness of a GC system normalized to the parent galaxy luminosity. Multicolor CCD data are available for NGC 4365 and NGC 4406 from Ajhar et al. (1994). These data were obtained on the KPNO 4 m telescope as part of a surface brightness fluctuation study and have a magnitude limit of about $V < 22.5$. We have applied the same 3 $\sigma$ rejection criterion to their GC data (kindly supplied by E. Ajhar) and find a mean color of $V-I = 1.10 \pm 0.01$ for 125 GCs in NGC 4365 and $V-I = 0.98 \pm 0.01$ for 96 GCs in NGC 4406. These colors are in very good agreement with those quoted in Table 2. Although their sample is smaller and has a brighter cutoff magnitude, it extends to slightly larger galactocentric distances. We have combined our sample with that of Ajhar et al. to show the radial variation

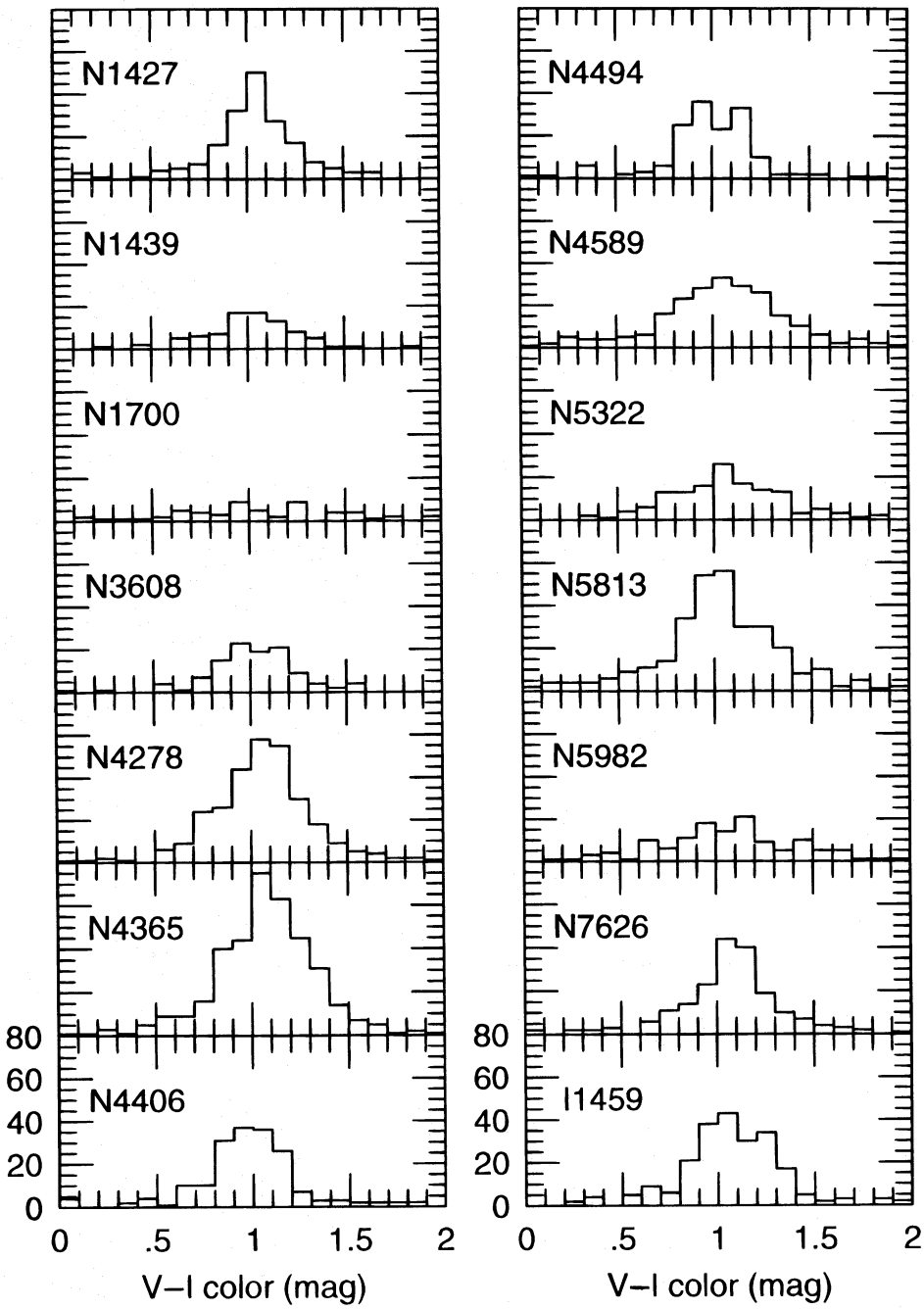


FIG. 6.—Histograms of globular cluster $V-I$ colors for the sample galaxies. The mean color for the combined sample is $V-I = 1.09$. Most galaxies reveal a fairly tight distribution, with two (NGC 4494 and IC 1459) showing evidence for a possible bimodal color distribution.

of GC color for NGC 4365 and NGC 4406 (see Fig. 12). Ajhar et al. concluded that there was little, or no radial gradient in either NGC 4365 or NGC 4406 GC colors. Our data extend the range to smaller radii and strengthen this conclusion.

### 4.2. *Magnitude Distribution*

Globular cluster luminosity functions (GCLFs) can help to constrain GC formation theories and have been used as standard candles for distance determination. Their use as a distance indicator is somewhat controversial, as it depends on the universality of the absolute magnitude of the turnover of the GCLF (see Harris 1991). It has been suggested that the turnover depends on metallicity (Ashman, Conti, & Zepf 1995) and the dispersion of the GCLF itself (Secker & Harris 1993). These issues, and an estimate of the Hubble constant from our GCLFs, will be considered in a future paper and are not discussed further here.

The variation of GC properties with galactocentric radius is of interest for formation and evolutionary theories of GCs. Although our data cover only a limited radial range (as set by the WFPC2 field of view), the central galaxy regions might be expected to show the most obvious signatures of some formation and destruction processes. For example, GC formation from two merging spirals may be expected to preferentially form new GCs in the inner regions (Ashman & Zepf 1992). The destruction processes, such as dynamical friction and tidal stripping, are negligible beyond $\sim 3$ kpc (provided GCs are not on highly radial orbits), so that GCs at these distances reflect their formation

TABLE 2

GLOBULAR CLUSTER PARAMETERS

| Galaxy (1) | Number of GCs (2) | $\langle V-I \rangle$ (mag) (3) | [Fe/H] (4) | $\Delta(V-I)/\Delta r$ (mag kpc$^{-1}$) (5) | $r_c$ (kpc) (6) |
|---|---|---|---|---|---|
| NGC 1427..... | 156 | $1.04 \pm 0.01$ | $-0.83 \pm 0.04$ | 0.0 | $1.2 \pm 0.2$ |
| NGC 1439..... | 86 | $1.04 \pm 0.01$ | $-0.83 \pm 0.07$ | 0.0 | $1.6 \pm 0.3$ |
| NGC 1700..... | 39 | $1.13 \pm 0.03$ | $-0.40 \pm 0.14$ | 0.0 | $2.7 \pm 1.6$ |
| NGC 3608..... | 96 | $1.00 \pm 0.01$ | $-1.06 \pm 0.05$ | 0.0 | $2.0 \pm 0.3$ |
| NGC 4278..... | 239 | $1.05 \pm 0.01$ | $-0.79 \pm 0.04$ | $-0.03 \pm 0.02$ | $0.95 \pm 0.1$ |
| NGC 4365..... | 328 | $1.10 \pm 0.01$ | $-0.55 \pm 0.04$ | 0.0 | $1.8 \pm 0.2$ |
| NGC 4406..... | 162 | $0.99 \pm 0.01$ | $-1.10 \pm 0.05$ | $-0.02 \pm 0.01$ | $2.3 \pm 0.4$ |
| NGC 4494..... | 139 | $1.04 \pm 0.01$ | $-0.84 \pm 0.06$ | $-0.04 \pm 0.01$ | $1.1 \pm 0.2$ |
| NGC 4589..... | 201 | $1.18 \pm 0.01$ | $-0.12 \pm 0.07$ | $+0.05 \pm 0.02$ | $1.5 \pm 0.2$ |
| NGC 5322..... | 148 | $1.16 \pm 0.01$ | $-0.22 \pm 0.07$ | 0.0 | $2.4 \pm 0.4$ |
| NGC 5813..... | 281 | $1.12 \pm 0.01$ | $-0.44 \pm 0.07$ | 0.0 | $2.8 \pm 0.4$ |
| NGC 5982..... | 113 | $1.12 \pm 0.02$ | $-0.44 \pm 0.08$ | 0.0 | $3.0 \pm 0.6$ |
| NGC 7626..... | 180 | $1.12 \pm 0.01$ | $-0.44 \pm 0.07$ | $-0.01 \pm 0.01$ | $4.0 \pm 0.7$ |
| IC 1459 ..... | 199 | $1.09 \pm 0.01$ | $-0.57 \pm 0.05$ | $-0.01 \pm 0.01$ | $2.5 \pm 0.4$ |
| Average ..... | 169 | 1.09 | $-0.62$ | ... | 2.1 |

NOTE.—(1) Galaxy name; (2) total number of globular clusters in the final list; (3) mean $V-I$ color and statistical uncertainty (after 3 $\sigma$ rejection criterion), corrected for Galactic extinction but not internal reddening; (4) mean metallicity from $V-I$ color; (5) gradient in $V-I$ color; (6) core radius of globular cluster system.

properties (Murray & Lin 1993). Interior to this, low-mass GCs may be subject to dynamical destruction processes (e.g., Aguilar, Hut, & Ostriker 1988).

The most notable feature of Figure 7 is that, for most galaxies, GC magnitude (and mass since the variation in mass-to-light ratio $[M/L]$ is expected to be small) does not vary with distance from the galaxy center. This uniformity is consistent with the formation scenarios of Harris & Pudritz (1994) and Vietri & Pesce (1995), although there is some evidence for a radial trend in our Galaxy (van den Bergh 1995a). As noted in § 3.2, small differences are seen for some galaxies.

### 4.3. *Color Distribution*

The color distributions for the whole sample between $0 < V-I < 2$ are shown in Figure 6 (which have been corrected for Galactic extinction but not internal reddening). The most obvious impression from Figure 6 is that the average globular cluster color does not vary much from galaxy to galaxy. As discussed in § 4.5, this is partly an effect of the limited range in galaxy luminosity for our sample. Most GCs have colors between $0.5 < V-I < 1.5$. Although the mean color does not depend on magnitude, the dispersion in color increases significantly at fainter magnitudes. Is the spread in GC colors intrinsic to the GC system (suggesting a range in GC metallicities), or is it simply due to photometric errors? We have compared the distribution of colors for the simulated GCs to those of the real GCs in NGC 4365 (a galaxy with no obvious dust and the richest GC system in our sample). We find that the dispersion in NGC 4365 GC colors is greater, particularly at bright magnitudes, than expected from simulations. Thus, although photometric errors play a role, there is some evidence that GC systems reveal an intrinsic range in color, and hence metallicity, within a single galaxy. This is also the situation from previous photometric and spectroscopic studies (see review by Harris 1991). Some galaxies have broad (NGC 4589 and and NGC 5813) or possible bimodal color distributions (NGC 4494 and IC 1459).

We note that Ajhar et al. (1994) found a wide range of color distributions for their 10 ellipticals. This is probably partly due to contamination by foreground stars and small background galaxies in their ground-based data. After applying a 3 $\sigma$ color selection to their data, we find that the galaxies with over 25 GCs have a mean $V-I$ color and dispersion of $1.07 \pm 0.04$ (NGC 3379), $1.10 \pm 0.01$ (NGC 4365), $0.92 \pm 0.02$ (NGC 4374), $0.98 \pm 0.01$ (NGC 4406), $1.08 \pm 0.01$ (NGC 4472), and $0.99 \pm 0.02$ (NGC 4552). So after excluding objects with extreme colors, the Ajhar et al. data set gives a similar result to ours, namely, a fairly uniform color distribution between GC systems.

Bimodal, or multimodal, color distributions are expected in the merger model for globular cluster formation of Ashman & Zepf (1992). During the early stages of the merger, a young, and initially blue, metal-rich GC population is formed. As this population ages, it rapidly reddens and, after about 1 Gyr, can be characterized as a relatively metal rich and red population of GCs. A bimodal metallicity distribution is seen in our Galaxy, with the metal-poor population associated with the halo and the more metal-rich with the disk. In this case, the bimodality may or may not have been the result of a merger. To date, the few detections of bimodal distributions in ground-based data of early-type galaxies have been somewhat controversial. Zepf & Ashman (1993) note that unimodal distributions can be ruled out in the Fornax cD galaxy NGC 1399, the dust lane elliptical NGC 5128, and the giant Virgo elliptical NGC 4472. In the case of NGC 4472, Ajhar et al. (1994) obtained a larger number of GCs compared to that available to Zepf & Ashman (1993), for which they described the $V-I$ color distribution as "uniform" between 0.85 and 1.30. Furthermore, Ajhar et al. found no visual evidence for bimodality in any of their other nine early-type galaxies, although they did not test for bimodality in a statistical way. Most recently, Geisler, Lee, & Kim (1996) present a still larger sample of GCs in NGC 4472, in which they report strong bimodality.

Elson & Santiago (1995) have presented WFPC2 data on GCs that lie $\sim 2'.5$ from the center of M87. Their $V-I$ color

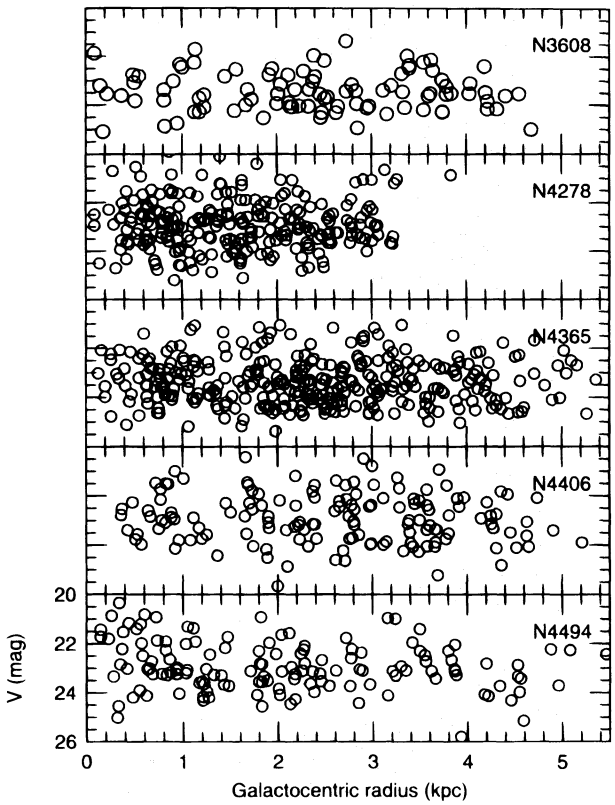


FIG. 7a

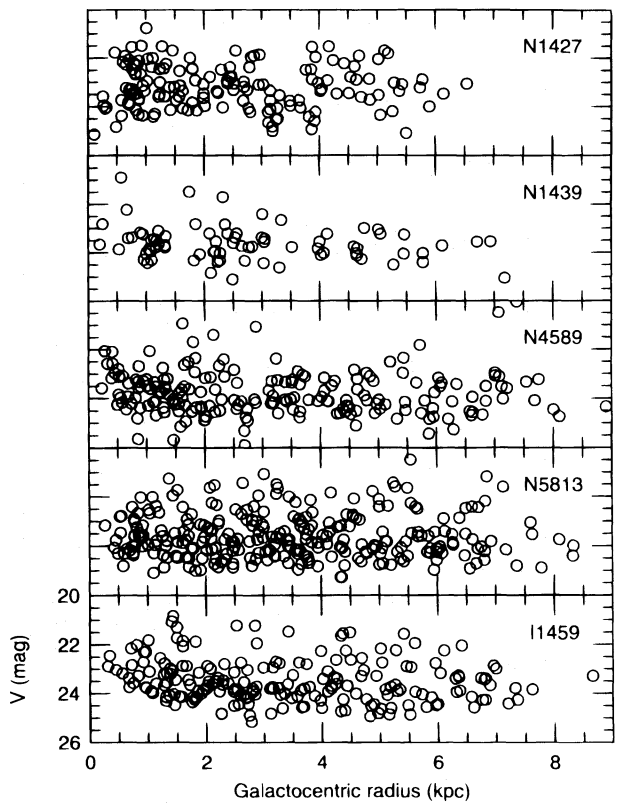


FIG. 7b

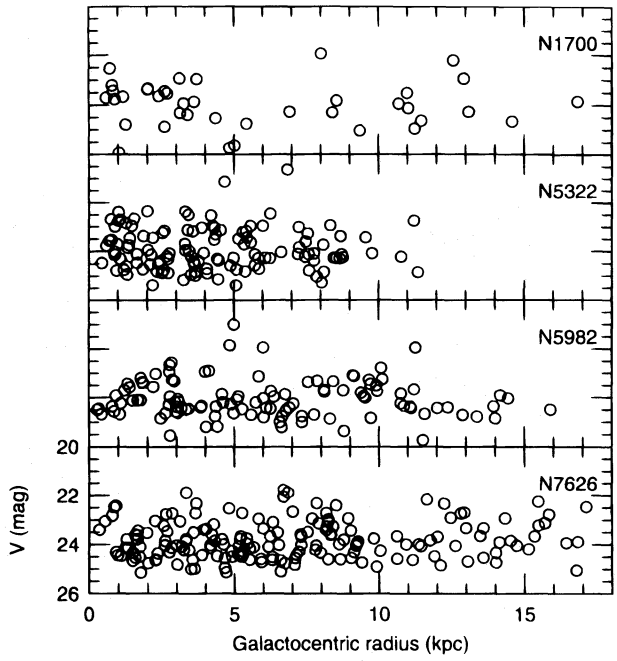


FIG. 7c

FIG. 7.—Globular cluster $V$ magnitude vs. galactocentric radius. The sample is ordered into nearby, intermediate, and more distant galaxies. For this and subsequent figures, we plot only globular clusters within 3 $\sigma$ of the mean color. Most galaxies show no radial gradient in the mean magnitude for the globular cluster system.

distribution reveals a striking bimodality contrary to that of previous ground-based data (Lee & Geisler 1993; Couture, Harris & Allwright 1990). In this case, the bimodality is supported by Whitmore et al. (1995) who studied GCs in the center of M87 with WFPC2. Neither Elson & Santiago nor Whitmore et al. discuss the radial distribution of their color subsamples.

The histograms of GC colors for our sample (Fig. 6) reveal a fairly symmetric distribution about a mean value, with two possible exceptions being NGC 4494 and IC 1459.

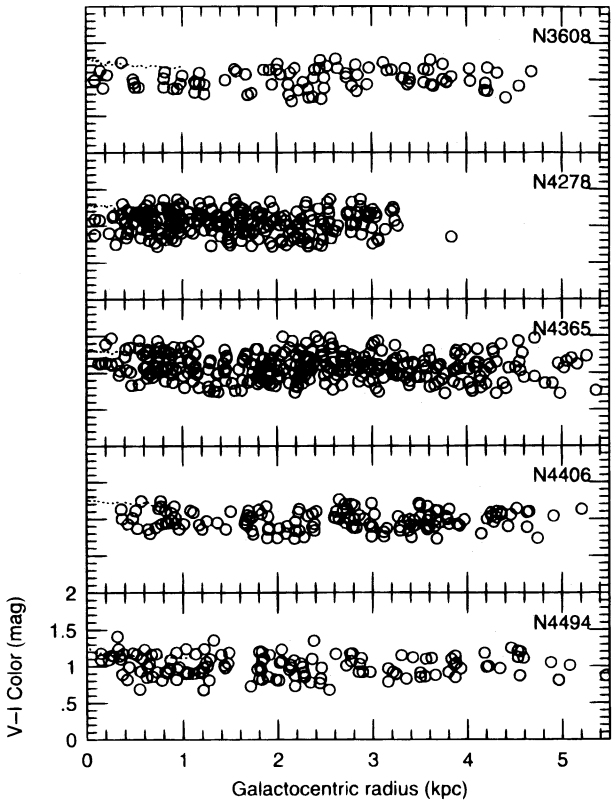


FIG. 8*a*

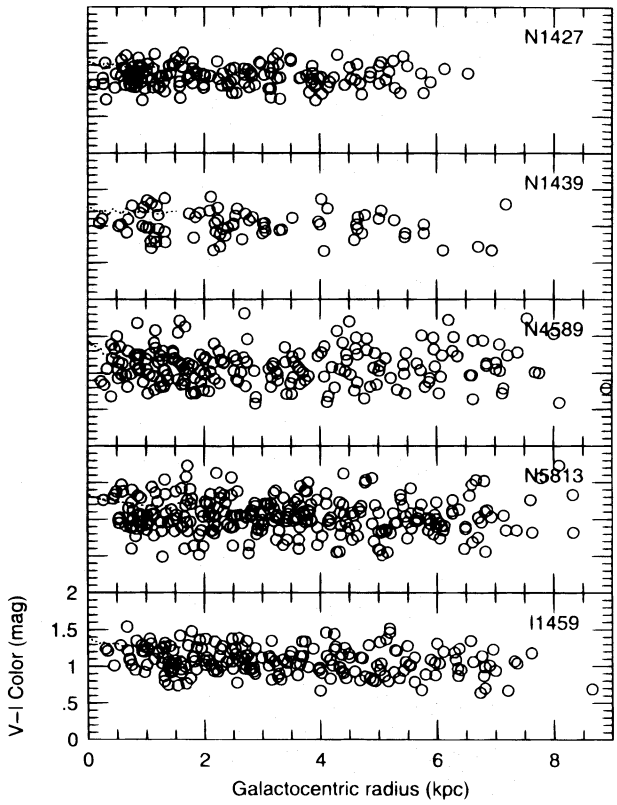


FIG. 8*b*

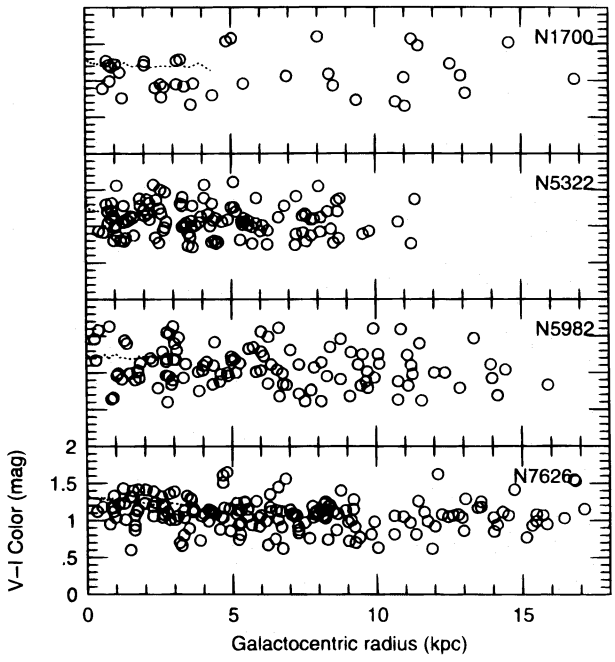


FIG. 8*c*

FIG. 8.—Globular cluster $V-I$ color vs. galactocentric radius. The sample is ordered as in Fig. 7. Galaxies reveal a weak, or no, radial color gradient for their globular clusters. We also show the $V-I$ color gradient (*dashed line*) for the underlying galaxy in the central kiloparsec from Carollo et al. (1996). In each case, the globular cluster mean color is bluer than the underlying starlight.

In order to quantify the color distributions, we have carried out a Hermite analysis, to $V = 24$, for all galaxies. This tests the distribution for non-Gaussian shapes. In no case do we find a statistically significant (i.e., $>3\ \sigma$) deviation from a Gaussian profile. So, although the color distributions for NGC 4494 and IC 1459 visually appear to be nonsymmetric, the effect is not statistically significant given, our sample size and errors. This does not rule out the possibility

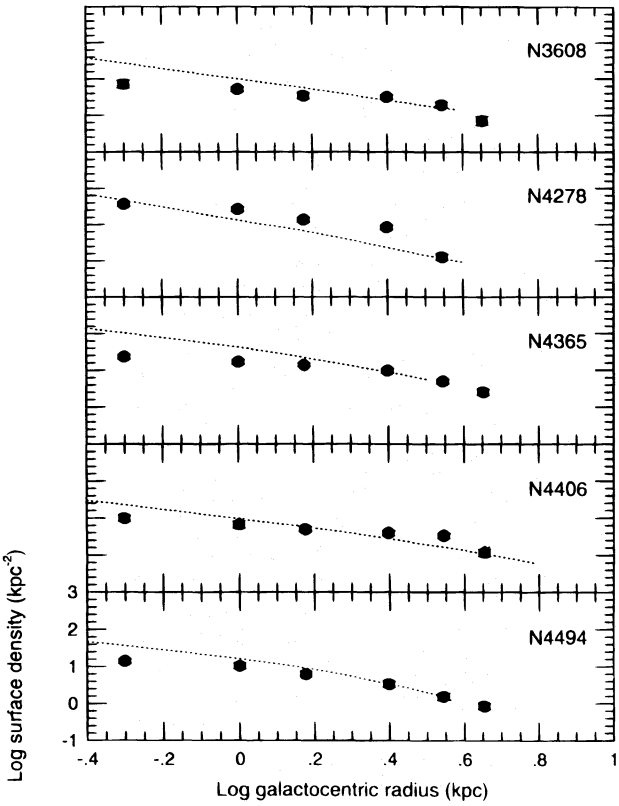


FIG. 9*a*

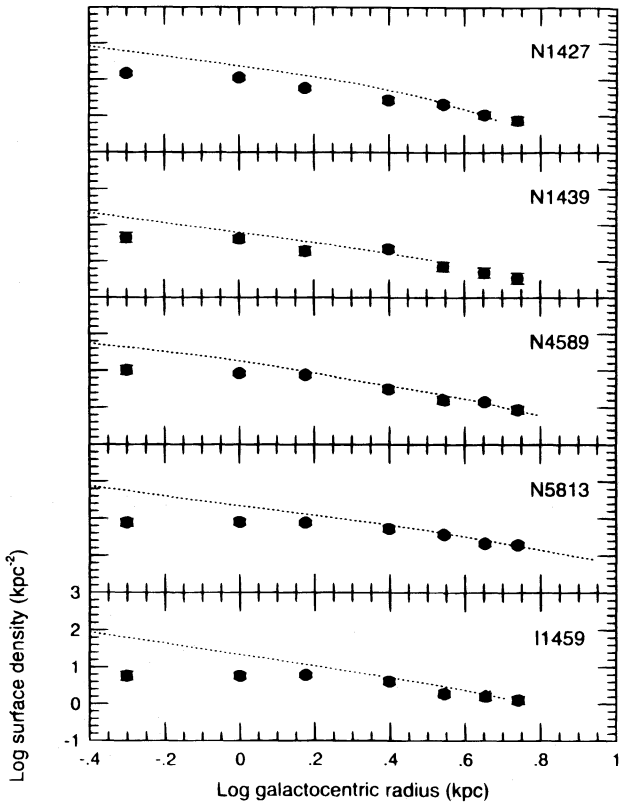


FIG. 9*b*

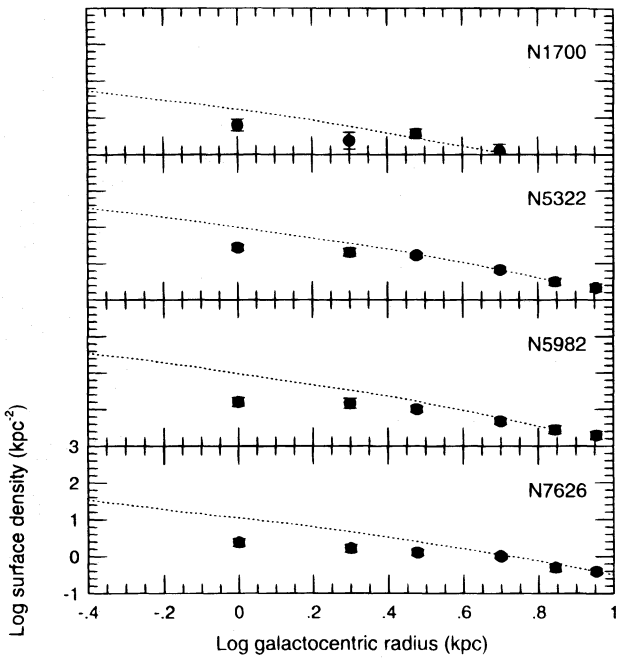


FIG. 9*c*

FIG. 9.—Globular cluster surface density vs. galactocentric radius. The sample is ordered as in Fig. 7. Error bars represent Poisson errors. The dashed line represents the underlying galaxy light normalized by an arbitrary offset. All galaxies reveal a turnover, or core, in the GC density distribution.

that with larger samples, deviations from a symmetric single-peaked Gaussian will be found. The two visual peaks are at $V-I \sim 0.95$ and 1.15 for NGC 4494, and $V-I \sim 1.05$ and 1.25 for IC 1459. Compared to the sample mean of $\langle V-I \rangle = 1.09$, the peaks in NGC 4494 straddle the mean, whereas for IC 1459 one peak is close to the mean value and the other appears to be an "additional" red population. In order to investigate the spatial location of these color subsamples, we have examined their distribution in polar coordinates, i.e., as a function of position angle and

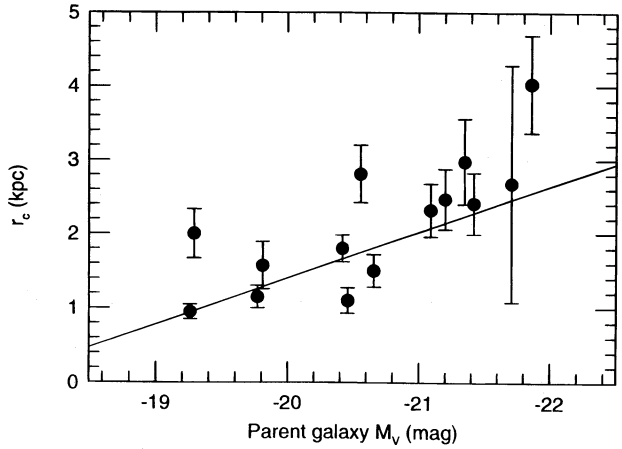


FIG. 10.—Core radius vs. parent galaxy luminosity. The solid line represents a weighted fit to the sample. More luminous galaxies tend to have more extended globular cluster systems.

radius. We have defined subsamples of $0.5 < V-I < 0.95$ and $1.15 < V-I < 1.6$ for NGC 4494, and $0.5 < V-I < 1.05$ and $1.25 < V-I < 1.8$ for IC 1459. For both galaxies, there is no strong trend with position angle nor galactocentric radius (i.e., the color subsamples are not centrally concentrated). To summarize, the current situation is that there is good evidence for bimodality in a small number of ellipticals, but many ellipticals show little or no evidence for bimodality. This may simply be due to the level of photometric errors or a limited number of GCs in each sample and remains an outstanding issue.

The results from ground-based data on radial gradients in GC properties have been summarized by Harris (1993). He concluded that for the Milky Way, M31, M104, M87, and NGC 5128 there is little evidence of color gradients for galactocentric distances beyond 4 kpc. However, definite gradients did exist for NGC 4472, NGC 4649, and NGC 1399 between 3 and 10 kpc. Our data probe, for the first time, regions less than 1 kpc from the galaxy center, and out to several kpc. Our sample galaxies have weak or nonexistent GC color gradients (see Fig. 8). Five galaxies show a slight reddening trend close to the galaxy center which could be due in part to dust at small radii. One galaxy, NGC 4589, suggests a blueing trend, but this is probably due to dust that is distributed throughout the galaxy even at large radii. Figure 13 shows a plot of $V-I$ color versus radius for the whole sample. Again only a weak, but not statistically significant, reddening trend is seen.

### 4.4. *Evidence for Young Globular Clusters?*

*HST* observations of NGC 1275 (Holtzman et al. 1992), NGC 7252 (Whitmore et al. 1993), and NGC 4038/4039 (Whitmore & Schweizer 1995), which are thought to have recently undergone a merger, reveal a population of bright ($V \sim 21$), blue ($V-I \sim 0.6$) semistellar objects. These blue objects tend to be centrally located and larger (by a factor of 2–3) than the red objects. Such characteristics suggest that they are young GCs formed in the merger of two gas-rich galaxies. On the other hand, van den Bergh (1995b) has argued that these objects are more like *open* rather than *globular* clusters.

Examination of Figure 5 in Whitmore et al. (1993) clearly reveals several bright, blue objects with many fewer red objects. Do we see evidence for a population of bright, blue and centrally located GCs in our sample? A quick visual inspection of the color maps in Carollo et al. (1996) shows straight away that we do not find a large population of such GCs. Ruling out a smaller population of faint, blue GCs in our sample is problematic due to the dust. As indicated in § 2.1, for nondusty galaxies such as NGC 4365, we detect the vast majority (~95%) of sources in the PC frame. Even for the galaxies with extensive dust (NGC 4278, NGC 4589, and IC 1459), the fraction of totally obscured GCs is probably not large given the relatively small covering fraction of dust.

We have inspected visually the PC image of each galaxy, searching by eye for any possible GCs not detected by DAOPHOT, particularly those along the edges of dust lanes. Although not objective, the eye is remarkably good at pattern recognition and detects approximately five faint, pointlike objects per galaxy that were not detected by DAOPHOT. These objects tend to be much more elongated than the detected GCs and have magnitudes $23 < V < 25$. They have a wide range of colors from very red to very blue, with an average color similar to that of the brighter detected GCs. There is no evidence for an extended blue tail in the color distribution of very faint objects. Indeed, their extreme colors can largely be explained by photometric errors at such magnitudes.

Thus, although there may exist a handful of genuine GCs with blue colors, they are not a dominant population at any magnitude or spatial location. Follow-up spectroscopy with 8–10 m class telescopes may be the only way to determine unambiguously whether the blue objects are young globular clusters.

### 4.5. *Metallicity Distribution*

In so far as $V-I$ color corresponds to metallicity, we have used the relation of Couture et al. (1990) to give the range in GC metallicity listed in Table 2. The mean metallicity of the whole sample is [Fe/H] = −0.62. The most metal-poor ([Fe/H] = −1.10) GC system is that of NGC 4406. The most metal-rich is that of NGC 4589, but the GC colors are probably reddened by the extensive dust present throughout the galaxy. For comparison, Milky Way GCs peak at [Fe/H] ~ −1.6 for halo GCs and −0.5 for disk GCs, with the ratio of halo to disk GCs being about 5:1. Thus, our elliptical galaxy GC systems have metallicities similar to those of spiral galaxy disk GCs and not spiral halo GCs. The weak radial color gradients seen in Figure 8 suggest also that the radial metallicity gradients are quite small, with the less metal-rich GCs at large distances. With a larger radial coverage, more convincing trends are seen in other galaxies, e.g., M87 (Lee & Geisler 1993). A strong metallicity gradient is indicative of dissipational collapse, although a gradient in the same sense is also expected in the Ashman & Zepf (1992) merger model.

In Figure 8, we show the variation of $V-I$ color for the GCs and the underlying galaxy in the central kiloparsec from Carollo et al. (1996). The systematic offset of $\Delta(V-I) \sim 0.10 \pm 0.02$ corresponds to a metallicity offset of $\Delta$[Fe/H] ~ 0.50 dex. This is in the sense that GCs are more metal poor than their parent galaxies at any given galactocentric distance. For the few GC systems studied to date, spectral metallicity determinations also give $\Delta$[Fe/H] ~ 0.5 dex between the GCs and the parent galaxy (Brodie & Huchra 1991; Harris 1991). Thus, the photometric and

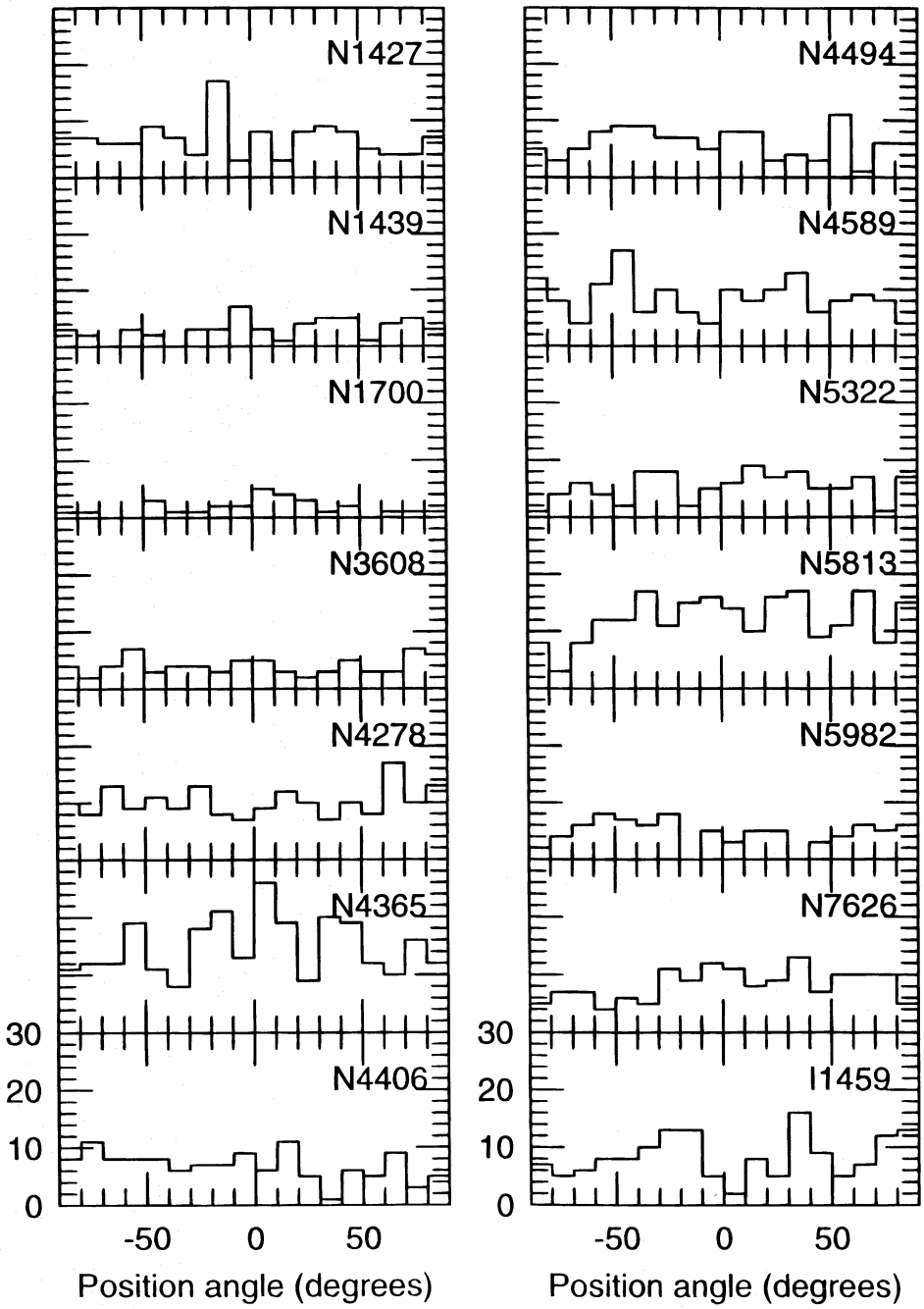


FIG. 11.—Histograms of globular cluster position angles for the sample galaxies after restricting the position angles to one hemisphere of the galaxy. The galaxy major axis is located at 0°.

spectroscopically derived metallicity determinations give similar values. These differences are consistent with a scenario in which GCs formed before the stars in their parent galaxy (though one cannot rule out subsequent formation from the low-metallicity gas).

It has been suggested that the mean metallicity of a GC system increases with the parent galaxy luminosity for all galaxy types (see, e.g., van den Bergh 1975; Brodie & Huchra 1991). This relation has been questioned by Ashman & Bird (1993) who suggest that no such correlation exists for nonspirals (they excluded ellipticals from their analysis) and that all halo GC systems have a mean metallicity of [Fe/H] $\sim -1.6$ irrespective of the parent galaxy luminosity. However, Perelmuter (1995) found that the dwarfs, spirals, and irregular galaxies *do* show a trend of metallicity with luminosity. Ellipticals are offset from this relation to higher mean metallicity for a given luminosity. This offset is interpreted by Perelmuter as a consequence of elliptical galaxies having formed by the merger of two spirals. The exact nature of the GC metallicity–galaxy luminosity relation has important implications for galaxy and GC formation, and these contradictory findings need to be resolved. A crucial ingredient in resolving this issue is to have a large sample of galaxies, particularly at intermediate luminosities, in order to explore the parameter space between dwarfs and massive galaxies. Of the previous studies, Brodie & Huchra (1991) had a sample of 10 galaxies, Ashman & Bird (1993) used seven, and Perelmuter

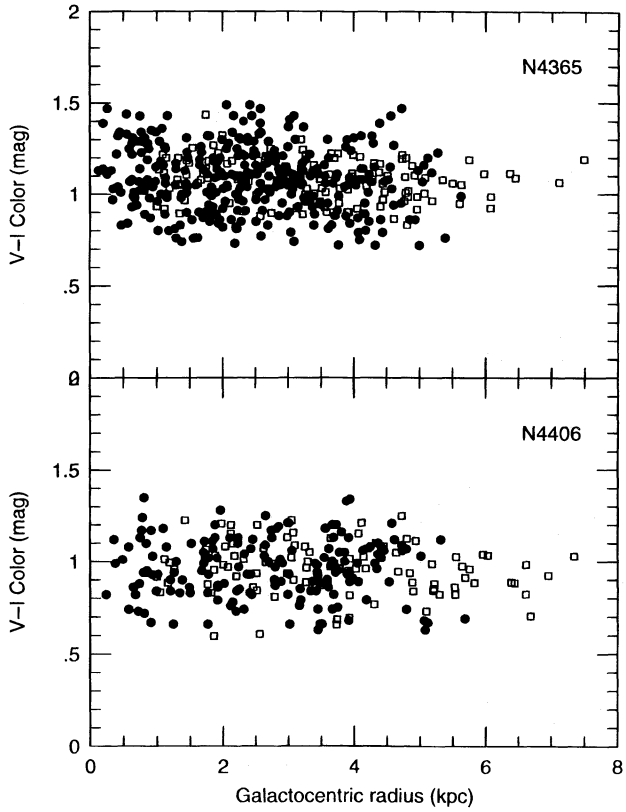


FIG. 12.—Globular cluster $V-I$ color vs. galactocentric radius for NGC 4365 and NGC 4406. Our sample is represented by filled circles and the ground-based data of Ajhar et al. (1994), after a 3 $\sigma$ color rejection, by open squares. For both galaxies, the two data sets are in good agreement.

(1995) had 17 galaxies. None of these studies had many galaxies with luminosities $-17 < M_V < -21$.

To further investigate this issue, we have combined the spectroscopic compilation of Perelmuter (1995) with metallicities for our sample and that of Ajhar et al. (1994), inferred from $V-I$ colors. This gives by far the largest total sample to date of 32 galaxies, with many at intermediate luminosities. The GC mean metallicity is plotted against parent galaxy luminosity ($h = 0.75$) for this combined sample in Figure 14. Data for NGC 4472 are plotted twice, giving both spectroscopic ([Fe/H] = −0.80) and photometric ([Fe/H] = −0.65) metallicities. Although there may be some offset in the photometrically versus spectroscopically determined metallicities, it is a relatively small effect. An important distinction from some earlier studies, is that we have subtracted off a disk component for the spirals using the mean bulge-to-disk ratios for different Hubble types given by Simien & de Vaucouleurs (1986). This gives an approximate bulge magnitude for each spiral galaxy that is probably more appropriate to use than the total galaxy luminosity, as most of our Galaxy's GCs are associated with the bulge. This is not practical for the SMC ($M_V = -16.9$) and the LMC ($M_V = -18.6$) for which we have used total luminosity. We have included new galaxies from Ajhar et al. (1994) that have more than 25 GCs after 3 $\sigma$ color rejection (i.e., NGC 3379, NGC 4374, and NGC 4552) but have excluded NGC 4589 as its GC colors are probably strongly affected by dust reddening. A weighted linear regression fit to the data points gives

$$[\mathrm{Fe/H}] = -0.17 \pm 0.01 M_V - 4.3 \, . \qquad (5)$$

We have not made any effort to ensure that the error bars are consistent between the different data sets nor to correct for any systematic offset between data sets, and so we cannot speculate about whether the scatter in the relation is intrinsic or not (however, for the luminous galaxies, the rms scatter appears to be ~0.4 dex in metallicity). However, we note that an unweighted fit gives a similar relation, i.e., [Fe/H] = $-0.16 \pm 0.02 M_V - 4.1$. For the fits we have used only the spectroscopically determined [Fe/H] for NGC 4472. Brodie & Huchra (1991) found a slope of

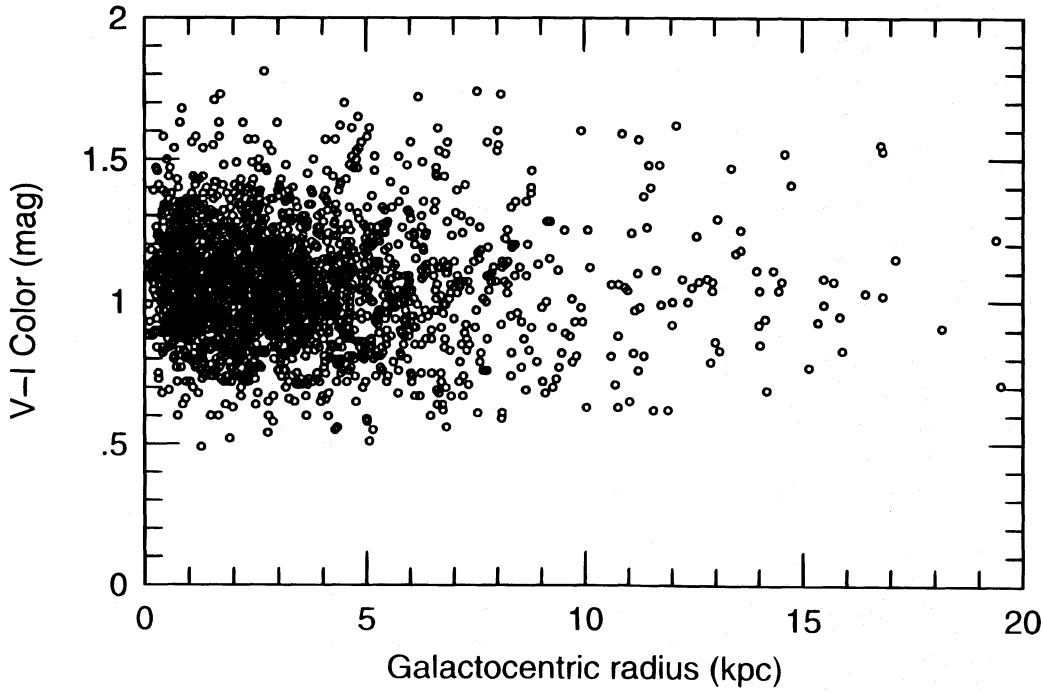


FIG. 13.—Globular cluser $V-I$ color vs. galactocentric radius for the combined sample. A weak reddening trend toward the galaxy center is seen.

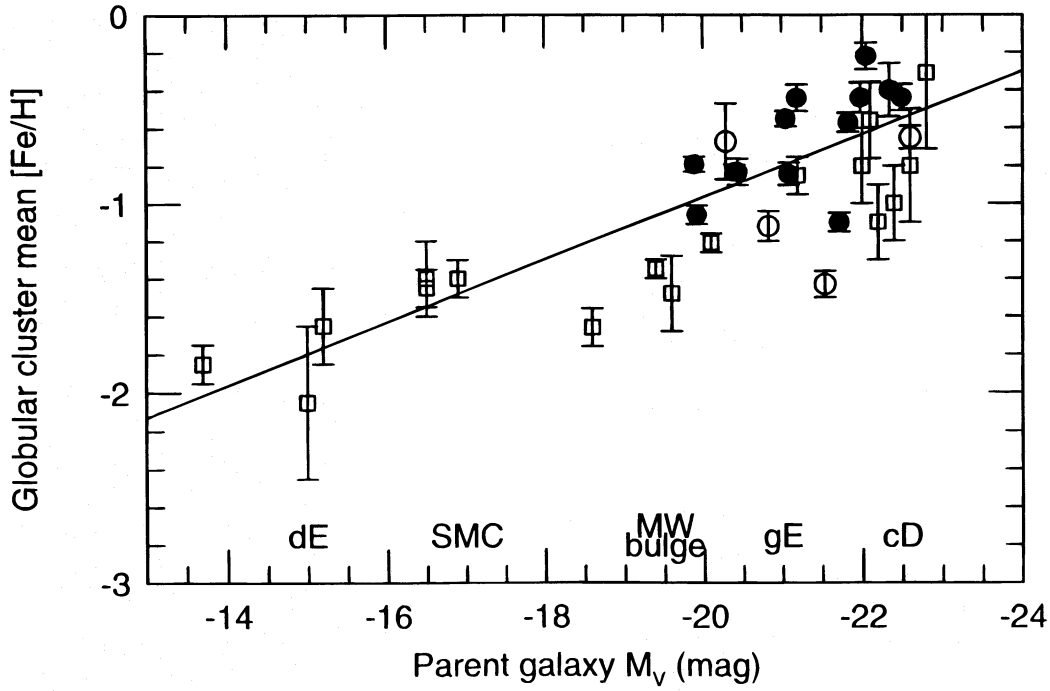


FIG. 14.—Mean globular cluster metallicity vs. absolute $V$ magnitude of the parent galaxy. Circles represent photometrically derived [Fe/H], and squares represent spectroscopically derived [Fe/H]. Our sample is given by filled circles, and the ground-based data of Ajhar et al. (1994) is shown as open circles. Spectroscopic metallicities are from the compilation of Perelmuter (1995). Although there may exist a small offset between photometric and spectroscopic metallicities, there is a strong correlation between the mean metallicity of the GC system and and the parent galaxy luminosity over several orders of magnitude. A weighted fit (shown by a solid line) gives $(Fe/H] = 0.17M_V - 4.3$. Realistic errors, within and between different data sets, are difficult to assess and so it is not clear if the scatter about the relation is intrinsic. A nonweighted fit gives a similar relation. For this plot we have assumed $h = 0.75$. The galaxies include dwarf ellipticals, the Magellanic Clouds, bulges of nearby spirals, and giant ellipticals.

$-0.13 \pm 0.02$ for a small sample of GC systems. The galaxies themselves obey a similar metallicity-luminosity relation, and for a large sample ($\sim 70$), Brodie & Huchra (1991) found the slope to be $-0.17 \pm 0.03$. Thus, with a larger number of GC systems, we find that the GC metallicity-luminosity relation has the same slope as the galaxy metallicity-luminosity relation, with a form of $Z \propto L^{0.4}$. This suggests that the same physical process governing gas enrichment occurred in both GCs and galaxies.

Da Costa & Armandroff (1995) have identified three or four GCs associated with the recently discovered Sagittarius dwarf spheroidal galaxy (Ibata, Gilmore, & Irwin 1994). The four GCs give an average metallicity of [Fe/H] = $-1.4$, and if we exclude the GC with a peculiar metallicity, the remaining three give [Fe/H] = $-1.8$. The correlation in Figure 14 would predict $M_V = -17.0$ to $-14.7$ for this range of metallicity. Costa & Armandroff suggest that it is around $M_V \sim -15$. So the GC system in the Sagittarius dwarf also appears to be consistent with the metallicity-luminosity correlation.

Ajhar et al. (1994) claim that there is a dependence of GC metallicity on environment in their data set. They point out that both NGC 4374 and NGC 4406, which lie close to the center of the Virgo Cluster potential well, have relatively blue (i.e., low-metallicity) globular clusters. Indeed, both these galaxies lie marginally below the locus of galaxies that have a similar luminosity in Figure 14, but given the uncertainty in photometrically versus spectrocopically derived metallicities, it would be premature to draw any conclusions at this stage.

To summarize, we find a correlation between GC system mean metallicity and parent galaxy luminosity (i.e., $Z \propto L^{0.4}$) over almost 10 mag, confirming the suggestion first made by van den Bergh (1975). The continuity appears to extend from dwarf ellipticals through the Magellanic Clouds and spiral bulges to giant ellipticals, unlike that seen in the smaller samples of Ashman & Bird (1993; there is no relation for dwarfs and spirals) and Perelmuter (1995 the relation exists only for spirals). This suggests a common origin for the GC populations over a large range of galaxy types. Although some type of metallicity-luminosity relationship would be expected in the merger of two spirals, it needs to be shown that such a merger will produce the type of relationship shown in Figure 14.

The work of Guzmán, Lucey, & Bower (1993) on the fundamental plane of spheroidal systems suggests that the only difference between dwarf and giant ellipticals is the relative scaling between the size of the initial dark halo and the size of the final light distribution. In particular, dwarf ellipticals obey the same luminosity-sigma and metallicity-sigma relations as giant ellipticals. Thus, qualitatively, we can explain the GC mean metallicity versus galaxy luminosity relation in terms of depth of the potential well and the galaxy's ability to retain metal-rich gas. The continuity in this relation from dwarf to giant ellipticals fits in well with the continuity seen in GC specific frequencies and the galaxy fundamental plane relations.

Although we cannot rule out alternatives at this stage, the similarity of the metallicity-luminosity relation for GCs and the galaxy stellar population, and the small offset to lower metallicity seen in GCs seems consistent with the idea that the majority of GCs in elliptical galaxies formed during a coalescence phase, perhaps shortly before the main epochs of star formation (see also Harris 1993).

### 4.6. *Surface Density Distribution*

Surface density profiles for our sample are shown in Figure 9. This figure indicates that the number of GCs per unit area rises less steeply than the underlying galaxy, i.e., it does not continue to rise as a power law. Such effects are difficult to see from ground-based data but have been seen in a few cases (see Harris 1991). Other *HST* studies find this effect also (e.g., Grillmair et al. 1994a).

All 14 of our sample galaxies reveal a turnover, or core, in their log surface density distribution. There are several effects which may give the appearance of a reduced rise in GC density in the inner regions: (1) a brighter limiting magnitude cutoff in the PC image, (2) changes in the GC luminosity function with radius, (3) obscuration due to dust, and (4) crowding of GCs. The first two possibilities do not appear to be significant, since our simulations showed no radial variation in magnitude, and the GC luminosity functions are consistent within sampling errors for GCs at small and large galactocentric distances. Furthermore, the detection fraction is similar from CCD to CCD, so that the detection characteristics in the PC image are similar to those in the WFC images. The third possibility cannot be ruled out, but the galaxies with no obvious dust (NGC 4365 and NGC 5982) also have clear surface density cores. Finally, even in the PC image, the density of GCs is not so high that they are blended together. So crowding can be ruled out. Thus, the cores seem to be real and typically have sizes of $r_c \sim 2$ kpc. In Figure 10 we show a correlation between core radius and galaxy luminosity. This correlation is in the sense that more massive ellipticals have larger core radii. Alternatively, the most luminous galaxies (i.e., those with $M_V \leq -21$) have large cores, but for the small, rotating ellipticals, the core radius is weakly, if at all, dependent on galaxy luminosity.

The Milky Way also shows a reduction in the surface density of GCs interior to about 1 kpc, and if we used the magnitude of the bulge it would lie close to the fit in Figure 10. The core in the Milky Way GC distribution has been attributed to destruction processes that have occurred after formation (e.g., Aguilar et al. 1988). However, in the case of NGC 3311, Grillmair et al. (1994a) concluded that the core radius of the distribution was too large to have been caused by dynamical friction even if operating for a Hubble time. Similar arguments can be made for the galaxies in our sample with the largest core radii. Furthermore, we do not expect dynamical friction, or tidal shocking, to produce a core radius with a steep dependency on galaxy mass as suggested by Figure 10. As destruction processes seem unlikely to explain the core distribution, the simplest explanation may be that the GC distribution is established at the epoch of formation.

### 4.7. *Azimuthal Distribution*

In Figure 11 we show the distribution of GCs as a function of position angle about the major axis. In several cases the GC distribution peaks close to the galaxy major axis. There are also notable exceptions, e.g., both NGC 4589 and IC 1459 have peaks close to 45° to the major and minor axes. For NGC 4406, there is a small enhancement at position angle $\sim -75°$ due to a companion (?) galaxy with its own small GC population. Combining the GC systems of all galaxies, we find a mean position angle that is consistent with the major axis of the galaxy itself (i.e., $3° \pm 15°$). This is also the case if we restrict the galaxies more elongated than E1 for which the position angle is better defined. The mean ellipticity is given by the quadrature sum of $\langle \sin 2\phi \rangle$ and $\langle \cos 2\phi \rangle$ for a radial density distribution of $\rho \propto r^{-2}$. This gives an average ellipticity for the GC systems of E0–E1, i.e., slightly rounder than the average galaxy light (see Table 1). The azimuthal distribution in a few other galaxies have been studied, e.g., M87 (McLaughlin, Harris, & Hanes 1994). McLaughlin et al. find that the GC system of M87 has a major axis that coincides roughly with the galaxy isophotes and has an ellipticity that increases with galactocentric distance, i.e., it is rounder near the galaxy center and flattens in the outer regions.

### 4.8. *Implications for Globular Cluster Formation*

In the last few years, quantitative information about extragalactic GC systems has grown rapidly. Such information now provides useful constraints on possible GC formation scenarios (Harris 1993). For example, correlations of GC properties with the parent galaxy would argue against a pregalactic origin for GCs, where GCs formed before the dark matter potential wells had assembled (see Peebles & Dicke 1968). Furthermore, the properties of GCs (e.g., kinematics, specific frequency, and metallicity) do not match those expected if they formed from a cooling flow (e.g., Harris, Pritchet, & McClure 1995; Grillmair et al. 1994b). In this subsection, we focus on the implications of our results, and those in the literature, for two general formation mechanisms. The first possibility is that GCs form at roughly the same epoch as the parent elliptical during the initial collapse at high redshift (e.g., Searle & Zinn 1978; Harris & Pudritz 1994). Alternatively, the merger of two spiral galaxies gives rise to an extended population of metal-poor GCs (Hernquist & Bolte 1993) and a centrally concentrated population of new metal-rich GCs (Ashman & Zepf 1992). We note that studies of nearby galaxies may only provide circumstantial evidence on the general problem of galaxy formation.

Starting with the latter, Zepf & Ashman (1993) have noted that their model can explain many of the observational constraints. In particular, they account for the shallower slope of the density profiles of GC systems as the "puffing up" of the metal-poor GC distribution. This gives rise also to a metallicity (and color) radial gradient that is offset to lower metallicity compared to the underlying galaxy at any given radius. Perhaps the clearest prediction of the Ashman & Zepf model is a bimodal metallicity (and hence color) distribution as discussed in § 4.3. The new metal-rich GCs are expected to be more centrally concentrated and at least as numerous as those of the original metal-poor GCs. Within the limitations of each GC system size (the richest system contained 328 GCs), we found no statistically convincing cases for a bimodal color distribution. Furthermore, the relative numbers of metal-rich to metal-poor GCs suggested by those distributions is ~1:1 and not 3:1 as might be needed to explain the large numbers of GCs seen in some ellipticals (see also van den Bergh 1995c). The number of ellipticals with clear bimodal metallicity distributions in the literature is small, and they tend to be massive ellipticals (too massive to be formed from two typical spirals). In our sample, we do not find evidence for a distinct red (metal-rich) population that is centrally concentrated. Although a population of young, blue GCs apears to have formed in several merging galaxies, there is little evidence to support the presence of such

objects in present-day ellipticals, even in those with unsettled dust distributions indicative of a recent accretion event. Perhaps the most interesting new results of this work that need to be understood in the context of the Ashman & Zepf (1992) merger model are the correlations of GC surface density core radius and GC mean metallicity with parent galaxy luminosity.

Similarly, no firm predictions exist for scenarios in which GCs form in an early collapse of unevolved galaxies, as most simulations of galaxy formation cannot yet resolve details at this level. The discussion therefore remains somewhat schematic and can be tested only for rough consistency. With these caveats, the differences between the GC density and metallicity profiles to those of the underlying galaxy can be understood if the GC system formed slightly earlier in the initial coalescence phase than the galaxy itself (see Harris 1993). Thus, for a given galaxy, GCs form in a more extended protogalaxy than the galaxy's stars, which results in a lower metallicity and more extended distribution for the GCs. For a virialized system, the variation in these properties is correlated with the depth of the potential well, which is in turn presumably related to the galaxy total luminosity. This scenario is similar to that envisaged by Eggen, Lynden-Bell, & Sandage (1962) and would suggest that the difference in metallicity at a given galactocentric radius (i.e., $\Delta$[Fe/H] $\sim$ 0.5 dex) corresponds to the timescale for galaxy collapse and star formation.

## 5. SUMMARY AND CONCLUSIONS

Very little is known about globular clusters in the central regions of elliptical galaxies, due to the effects of seeing/crowding on a bright galaxy background, in current ground-based observations. These problems are largely overcome using *HST*, which has the additional advantage that the effective contamination from foreground stars and background galaxies is very small. From WFPC2 imaging, we have identified globular clusters in the central few kpc of 14 elliptical galaxies with kinematically distinct cores (generally thought to be the result of an accretion of a gas-rich galaxy). These regions, close to the galaxy center, are where we expect to see the strongest signatures of some formation and destruction processes. Our sample increases substantially the number of extragalactic globular clusters systems studied to date.

After subtracting the background galaxy, we have used DAOPHOT to detect globular cluster candidates. We then measure sizes and magnitudes for these objects. Objects close to hot pixels, or those with extreme colors or large sizes, are removed from the candidate list giving $\sim$200 objects per galaxy, the vast majority of which are globular clusters. We have determined accurate positions, $V$ magnitudes, $V-I$ colors, and the spatial distribution of these globular clusters to a limiting magnitude of $V \sim 25$. The globular cluster sample is complete to $V \sim 24$. Comparison with the $V \leq 22.5$ KPNO 4 m observations of Ajhar et al. (1994) show good agreement for the two galaxies in common.

Before examining the magnitude, color, and spatial distribution of our sample globular clusters, we performed simulations to ensure that any trends seen were real and not simply some selection effect. In confirmation with previous ground-based studies, we find little or no trend for the globular cluster luminosity (and therefore mass, since changes in $M/L$ are expected to be small) to vary with distance from the galaxy center (galactocentric radius). Although we derive luminosity functions, we defer their discussion and any implications for the Hubble constant to a future paper. We find that the mean globular cluster color is remarkably constant with magnitude and that the spread in color, at any given magnitude, is intrinsic to the GC system. The fact that the mean color is very similar from galaxy to galaxy (i.e., $\langle V-I \rangle = 1.09 \pm 0.01$) probably reflects the small range in galaxy luminosity for our sample. Some galaxies show a weak reddening trend at small galactocentric radii, suggesting that globular clusters in the inner region are relatively more metal rich than those further out. This effect does *not* appear to be due to dust, but we cannot rule it out. Many galaxies are consistent with no radial globular cluster color gradient. For all sample galaxies, the globular cluster colors are bluer (more metal poor) than the underlying galaxy starlight at any given galactocentric radius. This difference, $\Delta(V-I) \sim 0.10 \pm 0.02$, corresponds to $\sim$0.5 dex in [Fe/H], which is consistent with that found spectroscopically for other galaxies (Brodie & Huchra 1991; Harris 1991).

Perhaps one of the most significant results from this work is the good correlation seen between globular cluster mean metallicity and parent galaxy luminosity. Such a relationship was suggested by van den Bergh (1975) and Brodie & Huchra (1991). We have increased significantly the number of galaxies in the relation by including photometrically derived metallicities for our sample and those from Ajhar et al. (1994), giving a total sample of over 30 spheroidal systems. The correlation implies that $Z \propto L^{0.4}$ over roughly 10 magnitudes, with a slope that is the same as that for the galaxy metallicity-luminosity relation. This continuity from dwarf ellipticals to spiral bulges to giant ellipticals provides a potentially interesting constraint on galaxy and globular cluster formation. In particular, we need to understand how giant ellipticals and their globular cluster population could form as the result of a merger of two typical spiral galaxies and reproduce the observed trend over many galaxy types and masses. We have also examined the radial and azimuthal distribution of globular clusters. We find that the surface density of globular clusters rises less steeply than the underlying galaxy light. Such an effect is not explained adequately by different completeness levels at small radii, dust obscuration, or blending of objects. A core model provides a good description to the radial surface density profile. More luminous galaxies in our sample have larger core radii, which would seem to rule out destruction of the globular clusters by dynamical friction as an explanation for the observed radial distribution. For most galaxies, the GCs are aligned closely with the galaxy isophotes, but they may have a slightly rounder distribution than the galaxy itself.

The correlations of globular cluster surface density core radius and mean metallicity with parent galaxy luminosity provide new constraints on models for the formation of globular clusters. We suggest that the properties of globular clusters are most consistent with their formation during the early collapse and coalescence phase at high redshift.

We thank J. Brodie and C. Grillmair for many useful discussions. We thank also the referee, S. van den Bergh, for his many suggestions, in particular noting the alternative interpretation of Figure 10. This research was funded by the *HST* grant GO-3551.01.91A.

## REFERENCES


Aguilar, L., Hut, P., & Ostriker, J. P. 1988, ApJ, 335, 720
Ajhar, E. A., Blakeslee, J. P., & Tonry, J. L. 1994, AJ, 108, 2087
Ashman, K. M., & Bird, C. M. 1993, AJ, 106, 2281
Ashman, K. M., Conti, A., & Zepf, S. E. 1995, AJ, 110, 1164
Ashman, K. M., & Zepf, S. E. 1992, ApJ, 384, 50
Balcells, M., & Quinn, P. J. 1990, ApJ, 361, 381
Baum, W. A., et al. 1995, AJ, 110, 2537
Bender, R., Burstein, D., & Faber, S. M. 1992, ApJ, 399, 462
Bender, R., & Surma, P. 1992, A&A, 258, 250
Bender, R., Surma, P., Dobereiner, C., & Madejsky, R. 1989, A&A, 217, 35
Brodie, J. P., & Huchra, J. 1991, ApJ, 379, 157
Burrows, C., et al. 1993, Hubble Space Telescope Wide Field and Planetary Camera 2 Instrument Handbook (Baltimore: STScI)
Carollo, C. M., et al. 1996, ApJ, submitted
Cohen, J. 1988, AJ, 95, 682
Couture, J., Harris, W. E., & Allwright, J. W. B. 1990, ApJS, 73, 671
———. 1991, ApJ, 372, 97
Da Costa, G. S., & Armandroff, T. E. 1995, AJ, 109, 2533
Eggen, O. J., Lynden-Bell, D., & Sandage, A. 1962, ApJ, 136, 748
Elson, R. A. W., & Santiago, B. X. 1996, MNRAS, in press
Fabian, A., Nulsen, P., & Canizares, C. 1984, Nature, 310, 733
Forbes, D. A., Elson, R. A. W., Phillips, A. C., Illingworth, G. D., & Koo, D. C. 1994, ApJ, 437, L17
Forbes, D. A., Franx, M., & Illingworth, G. D. 1995, AJ, 109, 1988
Forbes, D. A., & Thomson, R. C. 1992, MNRAS, 254, 723
Geisler, D., Lee, M. G., & Kim, E. 1996, AJ, submitted
Goudfrooij, P., Hansen, L., Jorgensen, H. E., & Norgaard Nielsson, H. U. 1994, A&AS, 105, 341
Grillmair, C. 1995, personal communication
Grillmair, C., et al. 1994a, AJ, 108, 102
———. 1994b, ApJ, 422, L7
Guzmán, R., Lucey, J. R., & Bower, R. G. 1993, MNRAS, 265, 731
Hanes, D. A. 1977, MmRAS, 84, 45
Harris, H. C., Baum, W. A., Hunter, D. A., & Kreidel, T. J. 1991, AJ, 101, 677
Harris, W. E. 1991, ARA&A, 29, 543
———. 1993, in ASP Conf. Ser. 48, The Globular Cluster-Galaxy Connection, ed. G. Smith & J. Brodie (San Francisco: ASP), 472
Harris, W. E., et al. 1986, AJ, 91, 822
Harris, W. E., Pritchett, C. J., & McClure, R. D. 1995, ApJ, 441, 120
Harris, W. E., & Pudritz, R. E. 1994, 429, 177
Harris, W. E., & van den Bergh, S. 1981, AJ, 86, 1627
Hernquist, L., & Barnes, J. E. 1991, Nature, 354, 210
Hernquist, L., & Bolte, M. 1993, in ASP Conf. Ser. 48, The Globular Cluster-Galaxy Connection, ed. G. Smith & J. Brodie (San Francisco: ASP), 788
Holtzman, J., et al. 1992, AJ, 103, 691
———. 1995a, PASP, 107, 156
———. 1995b, PASP, 107, 1065
Ibata, R. A., Gilmore, G., & Irwin, M. J. 1994, Nature, 370, 194
Illingworth, G. D., & Franx, M. 1989, in Dynamics of Dense Stellar Systems, ed. D. Merritt (Cambridge: Cambridge Univ. Press), 13
Lee, M. G., & Geisler, D. 1993, AJ, 106, 493
McLaughlin, D. E., Harris, W. E., & Hanes, D. A. 1994, ApJ, 422, 486
Mould, J. 1984, PASP, 96, 773
Murray, S. D., & Lin, D. N. C. 1993, in ASP Conf. Ser. 48, The Globular Cluster-Galaxy Connection, ed. G. Smith & J. Brodie (San Francisco: ASP), 738
Peebles, P. J. E., & Dicke, R. H. 1984, ApJ, 277, 470
Perelmuter, J. 1995, ApJ, 454, 762
Phillips, A. C., et al. 1995, in preparation
Roberts, M. S., Hogg, D. E., Bregman, J. N., Forman, W. R., & Jones, C. 1991, ApJS, 75, 751
Searle, L., & Zinn, R. 1978, ApJ, 437, 214
Secker, J., & Harris, W. E. 1993, AJ, 105, 1358
Schweizer, F. 1987, in Nearly Normal Galaxies, ed. S. Faber (New York: Springer-Verlag), 18
Simien, F., & de Vaucouleurs, G. 1986, ApJ, 302, 564
Stetson, P. B. 1987, PASP, 99, 191
van den Bergh, S. 1975, ARA&A, 13, 217
———. 1990, in Dynamics and Interactions of Galaxies, ed. R. Wielen (Berlin: Springer-Verlag), 492
———. 1995a, AJ, 110, 1171
———. 1995b, ApJ, 450, 27
———. 1995c, AJ, 110, 2700
Vietri, M., & Pesce, E. 1995, ApJ, 442, 618
Whitmore, B. C. 1995, private communication
Whitmore, B. C., & Schweizer, F. 1995, AJ, 109, 960
Whitmore, B. C., Schweizer, F., Leitherer, C., Borne, K., & Robert, C. 1993, AJ, 106, 1354
Whitmore, B. C., Sparks, W. B., Lucas, R. A., Macchetto, F. D., & Biretta, J. A. 1995, ApJ, 454, L73
Zepf, S. E., & Ashman, K. M. 1993, MNRAS, 264, 611